

AD-756 254

CONDUCTION MECHANISMS IN THICK FILM  
MICROCIRCUITS

R. W. Vest

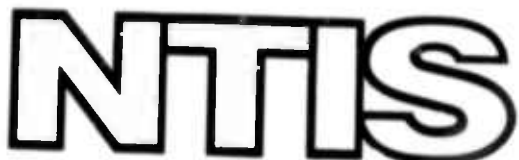
Purdue Research Foundation

Prepared for:

Advanced Research Projects Agency

1 February 1973

DISTRIBUTED BY:



National Technical Information Service  
U. S. DEPARTMENT OF COMMERCE  
5285 Port Royal Road, Springfield Va. 22151

AD 756254

Semi-annual Technical Report  
for the Period 7/1/72 - 12/31/72

Conduction Mechanisms in Thick  
Film Microcircuits

Grant Number: DARC15-70-G7

ARPA Order No.: 1642

Grantee: Purdue Research Foundation

Principal Investigator: R. W. Vest  
(317) 749-2601

Effective Date of Grant: 7/1/70

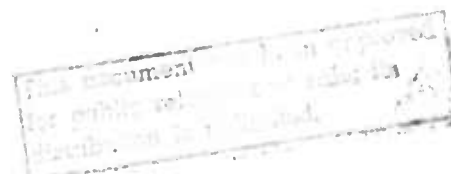
Grant Expiration Date: 6/30/73

Amount of Grant: \$181,260

February 1, 1973

Reproduced by  
NATIONAL TECHNICAL  
INFORMATION SERVICE  
U S Department of Commerce  
Springfield VA 22151

Details of illustrations in  
this document may be better  
studied on microfiche



D D C  
SEARCHED  
INDEXED  
FEB 21 1973  
B

### Forward

The research described in this report constitutes the fifth six months effort under a grant from the Advanced Research Projects Agency, Department of Defense under the technical cognizance of Dr. Norman Tallan, Aerospace Research Laboratories, United States Air Force. The research was conducted in the Turner Laboratory for Electroceramics, School of Electrical Engineering and School of Materials Science and Metallurgical Engineering, Purdue University, West Lafayette, Indiana 47907, under the direction of Professor R. W. Vest. Contributing to the project were Assistant Professor G. L. Fuller, Mr. D. J. Deputy, Mr. E. M. Miller, Mr. A. N. Prabhu, Mr. T. R. Raghunath, Mr. R. L. Reed, and Mr. J. L. Wright.

Abstract

Results from studies of the resistance of RuO<sub>2</sub>-glass resistors during firing and of the surface tension of the glass are presented, and their correlation with the proposed model for microstructure development discussed. Studies of the removal of the ethyl cellulose - butyl carbitol screening agent led to the conclusion that the last traces of organic materials cannot be removed below 500°C. An investigation of the drying of RuO<sub>2</sub> · xH<sub>2</sub>O employing DTA and TGA techniques is discussed, and a procedure described for preparing anhydrous RuO<sub>2</sub> with suitable particle size range.

## TABLE OF CONTENTS

	<u>Page</u>
I. Introduction	1
II. Microstructure Development Studies	3
A. General	3
B. Apparatus	4
1. Resistivity During Firing	4
2. Surface Tension	4
3. Neck Growth	8
C. Experimental Procedure	8
1. Resistivity During Firing	13
2. Surface Tension	13
D. Results	14
1. Resistivity During Firing	15
2. Surface Tension	15
3. SEM Studies	22
	28
III. Screening Agent Removal	30
A. General	30
B. Apparatus	31
C. Procedure	33
D. Results	33
IV. RuO <sub>2</sub> Power Preparation	40
A. General	40
B. Procedure	41
C. Results	41
V. Summary and Future Plans	48
VI. References	54
VII. Distribution List	55

## LIST OF FIGURES

<u>Figure</u>		<u>Page</u>
1	Resistance and Temperature Measuring System	5
2	Resistance Sense Amplifier	7
3	Surface Tension Apparatus	9
4	Metallograph with Video Cameras	10
5	Metallograph Hot Stage	12
6	Resistance versus Time of Sample 35	17
7	TCR versus Time of Sample 35	18
8	Temperature and Thermal History Dependence of Sample 35	20
9	Surface Tension of Lead-Silicate Glass	23
10	Surface Tension of Lead Borosilicate Glass	25
11	Effects of Surface Tension on Resistor Formation	26
12	Scanning Electron Micrographs of Etched Resistors	29
13	Thermogravimetric Analysis Apparatus	32
14	Isothermal Evaporation Rate of Butyl Carbitol versus Reciprocal Temperature.	35
15	Isothermal Evaporation Rate of Screening Agent	36
16	Evaporation of Screening Agent at Constant Heating Rate	38
17	Differential Thermal Analysis of the Dehydration of $\text{RuO}_2 \cdot x\text{H}_2\text{O}$	42
18	Weight Loss of $\text{RuO}_2 \cdot x\text{H}_2\text{O}$ at Constant Heating Rate	44
19	Scanning Electron Photomicrographs of Dried $\text{RuO}_2$ Powder	46

## I. Introduction

The current status of thick film technology as applied to conductive and resistive formulations is largely the result of empirical developments. The development of new materials as well as the improvement of existing systems have been hindered by an inadequate understanding of the mechanisms by which electric charge is transported in thick film resistors and conductors.

One of the factors that any model for conduction in thick film microcircuits must explain is the fact that the temperature coefficient of resistance (TCR) of a resistor is much lower than the TCR of any of the individual ingredients from which it was made. Several possible approaches to explaining this "TRC anomaly" which are being explored in this project are:

1. Changes in contact resistance between adjacent particles due to thermal stresses,
2. Changes in the intrinsic properties of the conductive material during processing,
3. Formation of new phases which contribute to the conduction,
4. Size effects which change the intrinsic properties of the conductive,
5. Changes in the geometry factor with temperature.

Published work concerning these possible mechanisms was discussed in the first report on this project [1].

The primary thrust of the experimental program is to relate the electrical properties of the thick films to the material properties and processing conditions through microstructure. The materials properties to be correlated are: resistivity; temperature coefficient of resistivity; coefficient of thermal expansion; interfacial energy; particle shape, size, and size distribution; and chemical reactivity with other constituents. The processing conditions to be correlated are time, temperature, and atmosphere during firing.

The specific objectives of the program are:

1. Determine the dominant sintering mechanisms responsible for microstructure development, and establish the relative importance of the various properties of the ingredient materials.
2. Determine the dominant mechanisms limiting electrical charge transport, and establish the relative importance of the various properties of the ingredient materials.
3. Develop phenomenological models to inter-relate the various material properties with system performance.

A proposed model to satisfy objective 1 above was presented in the previous report [2], and the microstructure development studies presented in this report have been developed to test the various aspects of the model. Results obtained to date are in general agreement with the predictions of the model. Several sub-projects pertaining to objective 2 have been discussed in previous reports [1, 2, 3, 4] and work is continuing along several lines, but a discussion of these results will not be presented until the next semi-annual report. Studies of RuO<sub>2</sub> power preparation and screening agent removal discussed in this report were undertaken in order to contribute to objective 3.

## II. Microstructure Development Studies

### A. General

This phase of the project is concerned with establishing a scientific understanding of the mechanisms of microstructure formation that exist during the firing steps of manufacturing. The formation of the microstructure is the most important event in the entire thick-film process, and establishing desirable control over manufacturing depends upon a proper level of understanding. A model for the sintering process developed in an earlier report [2] predicts a sequence of glass sintering, conductive network formation, and final densification. Part of the value of this model is that it suggests experiments that can be performed to test its validity.

One set of experiments involves the continuous measurement of resistance during the firing of  $\text{RuO}_2$  - glass thick film resistors. The intentions of these studies are four-fold: (1) to determine the onset of electrical continuity as a function of temperature at various heating rates for correlation with the sintering model; (2) to determine the onset of electrical continuity as a function of time at various temperatures for correlation with the sintering model; (3) to determine the resistance as a function of time at elevated temperatures in order to study the proposed ripening process; and (4) to prepare resistors at known stages of the firing process for subsequent microstructural investigation by SEM and optical techniques.

The dominant sintering mechanisms responsible for the microstructure development can be directly studied either by measuring the neckgrowth between two adjacent particles or by determining the overall shrinkage as a

function of time and temperature. Since this system involves a major fraction of glass, it is difficult to perform shrinkage measurements at temperatures much beyond the softening temperature of the glass; therefore, only neckgrowth studies are suitable. Most previous neckgrowth studies of sintering phenomena have been carried out by quenching from elevated temperatures with subsequent examination by metallographic techniques. However, only a limited picture of the actual changes can be obtained from such room temperature observations, and hot stage microscopy will be employed to study the neckgrowth between spheres as a function of time and temperature.

The sintering model predicts that the driving force for conductive network formation is directly proportional to the surface tension of the glass. It is therefore essential to accurately measure the surface tension as a function of temperature and impurity content. These studies have been initiated, and results to date are discussed.

## B. Apparatus

### 1. Resistivity During Firing

The apparatus used for electrically monitoring the formation of resistors during firing is the push rod furnace described earlier [1]. The resistance and temperature measuring system used with the furnace, shown as a block diagram in Figure 1, has been modified in order to measure higher values of resistance encountered in firing resistors with low concentrations (5-10%) of  $\text{RuO}_2$ . The current in the sample from the 1000Hz sinusoidal source,  $V_s$ , is limited by  $R_s$ . One of the two preamplifiers and the tuned amplifier sense the voltage across the potential terminals of the sample, and the rectified, quasi-dc, voltage drives a three decade chart recorder;  $R_{C1}$  and  $R_{C2}$  represent lead wire resistance and the

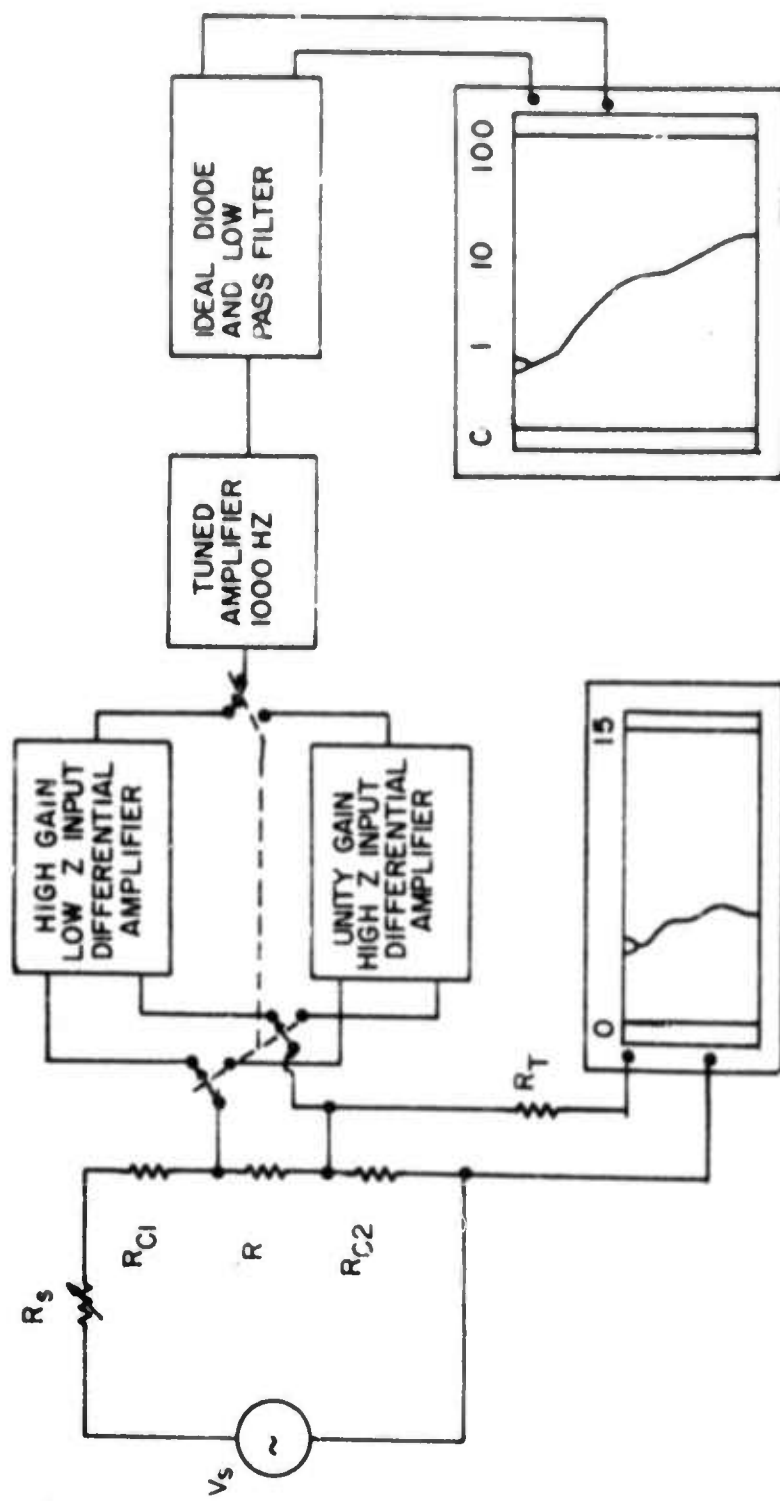


Figure 1  
Resistance and Temperature Measuring System

resistance of the sample up to the potential terminals. In four terminal measurements the lead wire resistances do not influence the determination of the resistance between the potential terminals,  $R_s$ , and for large resistance samples where  $R_{C1}$  and  $R_{C2}$  are negligible, two terminal measurements may be used. Sample temperature is determined with a platinum - platinum + 10% rhodium thermocouple that is part of the four leads to the resistor. The dc thermal emf and the ac resistance measuring voltage are easily separated and do not influence one another. The sense amplifier for resistance measurements is shown in greater detail in Figure 2. The original sense amplifier, consisting of op-amps A1, A4, A5 and A6 and associated components, has been modified by adding a second preamplifier, suitable for high impedance samples, that can be substituted for the lower impedance preamplifier using A1. The new preamplifier, using A2 and A3 with junction field effect transistor input stages and the 10 Megohm feedback and input resistors of the standard differential amplifier configuration, has a 20 Megohm input impedance at the plus terminal and a voltage gain of 1. The circuit consisting of A3, 1100 pf, and two fixed resistors and one potentiometer is a standard variable negative capacitance circuit. Its purpose is to cancel the circuit capacitance which consists mostly of cable capacitance from the sample to the amplifier input. If the total capacitance becomes negative the preamplifier circuit will oscillate so the net capacitance is adjusted to + 15 pf. The reactance of 15 pf at 1000 Hz is about 10 megohms, and as long as  $R_s$  in Figure 1 is less than or equal to 1 megohm this reactance causes negligible error. By considering the noninfinite impedance of the measuring circuit it is possible to make resistance measurements in excess of 20 megohms.

The value of  $R_s$  and the magnitude of  $V_S$  of Figure 1 depend on the

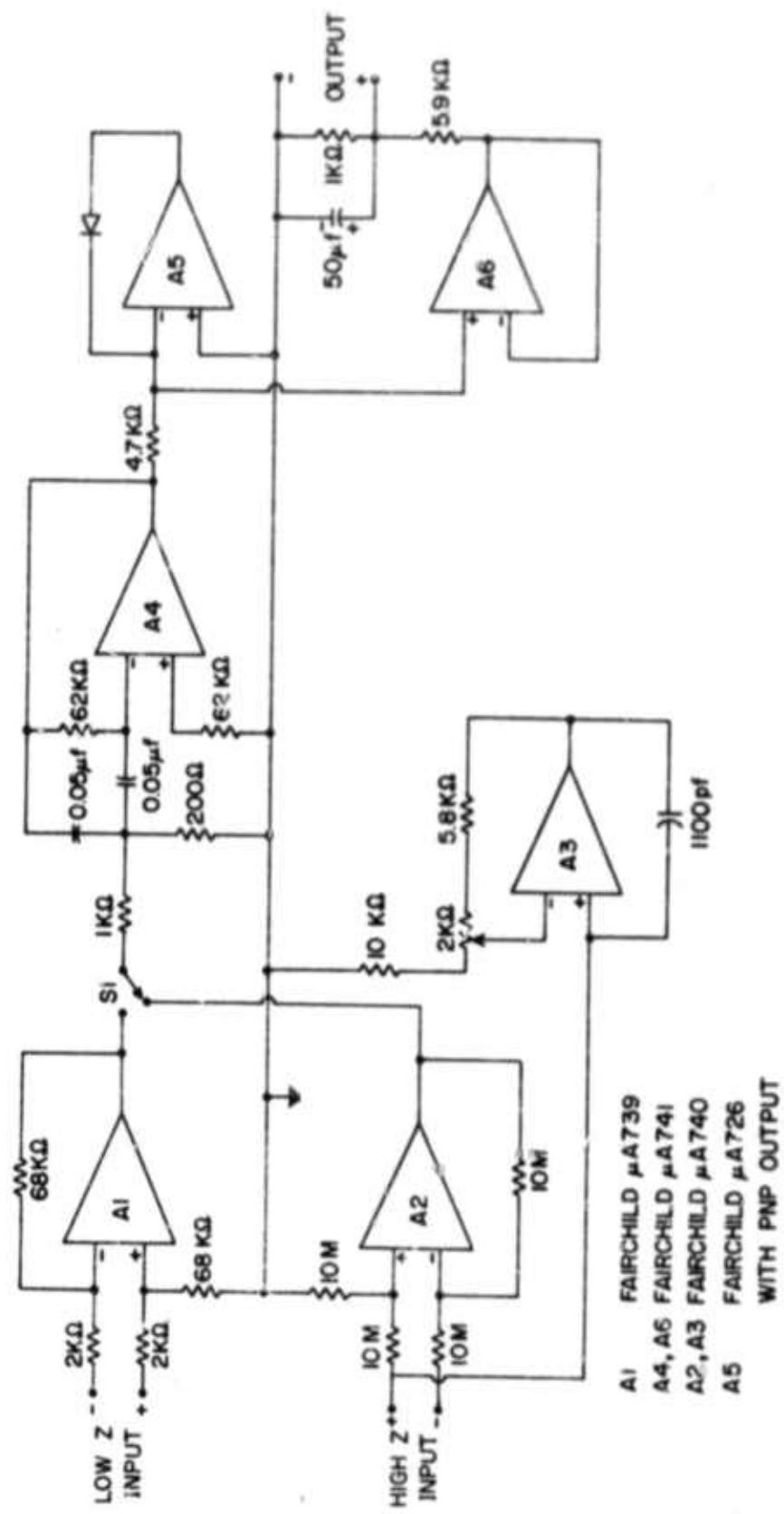


Figure 2  
Resistance Sense Amplifier

sample resistance. For low resistance samples  $V_S$  and  $R_S$  are made large so that they approximate a constant current source. Under these conditions the deflection of the chart pen is directly related (proportional within each decade) to the sample resistance. When sample resistances are very large during some portion of the experiment the oscillator voltage is decreased so that the pen is on-scale for an infinite sample resistance and  $R_S$  is then selected for the best sensitivity over some range of resistance. Sample resistances are always determined by comparing them to standard resistors rather than by determining  $V_S$  and the gain of the amplifier.

## 2. Surface Tension

The surface tension of the glass used in other phases of this project has been measured with a modified dipping platinum cylinder method using the apparatus shown in Figure 3. A platinum cylinder, 0.5 inches in diameter, 0.5 inch high, and 0.005 inches thick, is suspended by a platinum hang down wire from an automatic recording Ainsworth micro-balance to be described later. A platinum crucible, 1 $\frac{1}{2}$  inches in diameter and 1 $\frac{1}{2}$  inches deep, is placed on a ceramic support so that it is centered in a tube furnace that can be raised or lowered by means of a labjack. The temperature of the glass in the crucible is measured by a chromel-alumel thermocouple placed in contact with the bottom of the platinum crucible.

## 3. Neck Growth

The neckgrowth between adjacent spherical particles during sintering will be observed with the modified metallograph shown in Figure 4. The entire optical portion of the metallograph has been inverted on the floating mounts so that the sample can be heated in an up-tight position

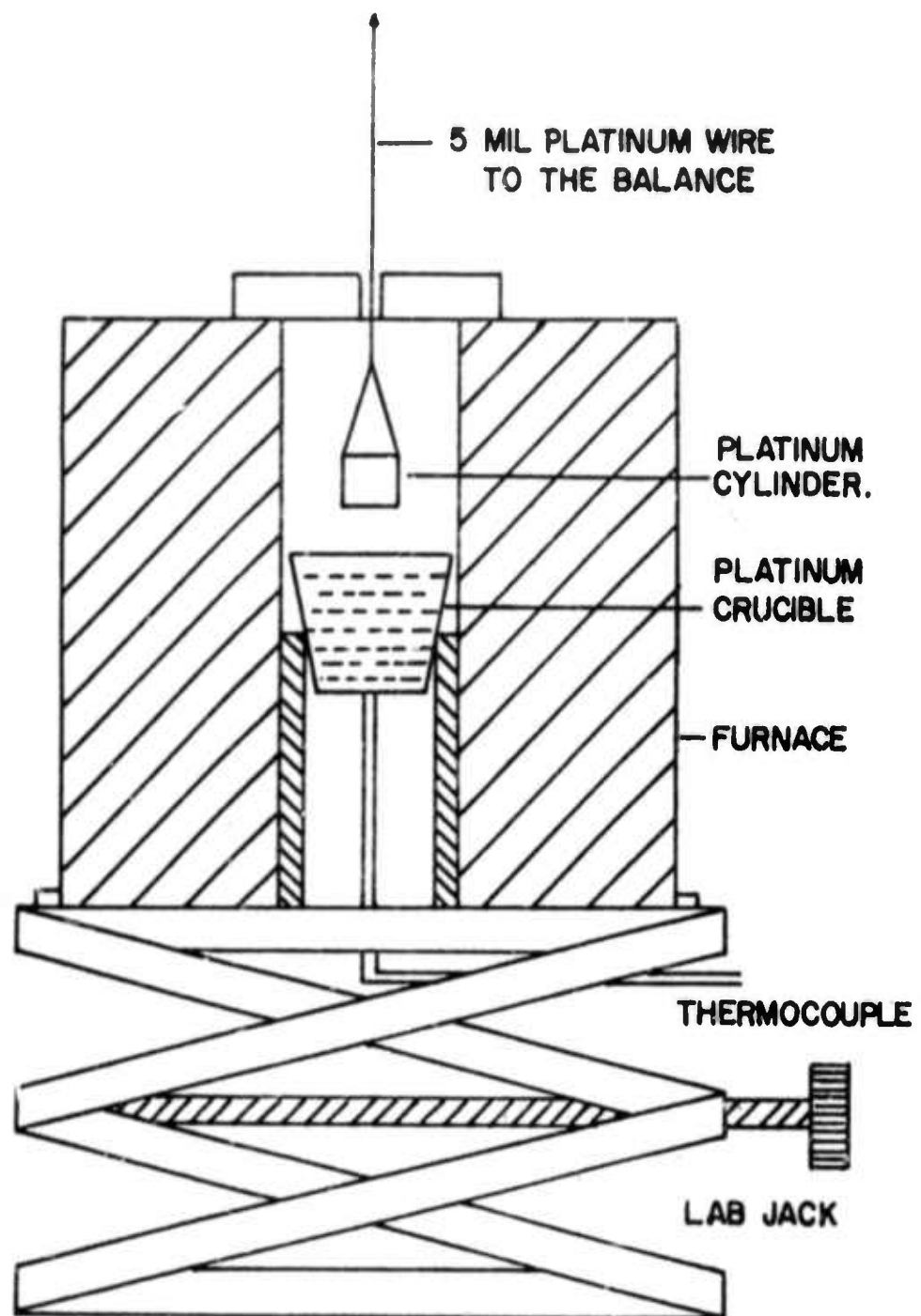


Figure 3  
Surface Tension Apparatus

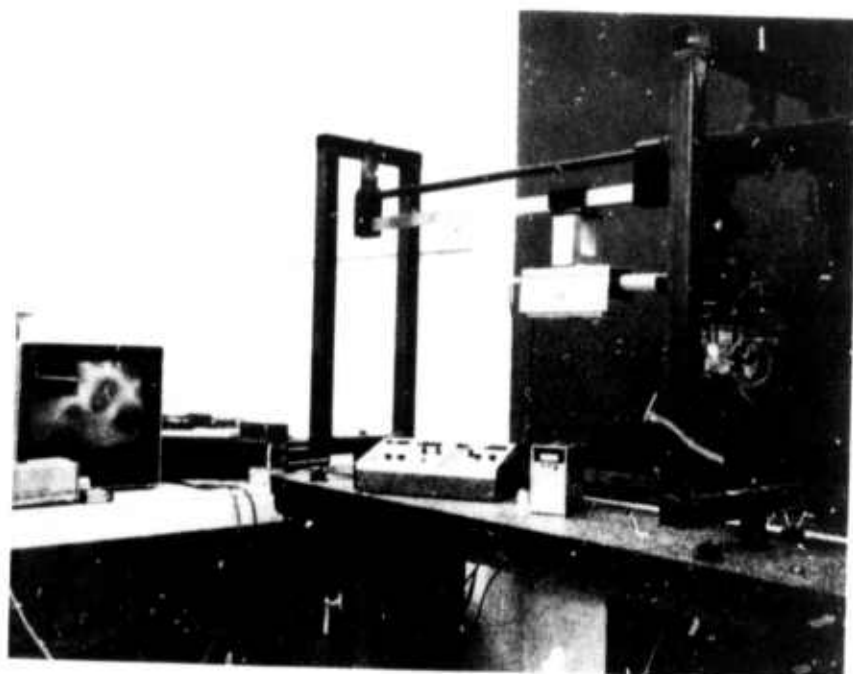


Figure 4. Metallograph with Video Cameras

and viewed from the top. The regular camera system has been removed and replaced by a Sony AUC-3200 black and white video camera. A second video camera is used to monitor a digital voltmeter that measures the sample thermocouple emf and a digital clock. A Sony special effects unit then mixes the two video signals so that the emf and time are positioned in a corner of the viewing area. All information thus obtained is recorded on a Sony AV-3600 video recorder with stop frame capability, and observed on a Conrac SNA television monitor.

The hot stage unit on which the samples will be heated is a Unitron MMS vacuum heating stage modified slightly as shown in Figure 5. It consists of water cooled upper and lower portions constructed of stainless steel which are bolted together and sealed with a thick rubber gasket that slightly separates the two portions; small holes in the gasket provide feed-throughs for thermocouples. The tungsten ribbon electric heater normally used in this unit has been replaced by a cylindrical heater consisting of 10 mil - platinum + 30% rhodium wire wound on a boron nitride core, 3/8" in diameter. This heater sits in the lower portion of the hot stage on a refractory base and is insulated with Fiberfrax contained in a larger refractory tube. The sample holder is a small platinum pan located on top of the boron nitride core, and platinel thermocouple leads are used to record the sample temperature. Another platinel thermocouple is positioned in the center of the boron nitride core and is used to control the temperature of the furnace. The sintering experiments will be carried out under both isothermal and constant heating rate conditions in order to quantitatively test the sintering model.

Since temperatures as high as 900°C will be employed, a 5 mil thick

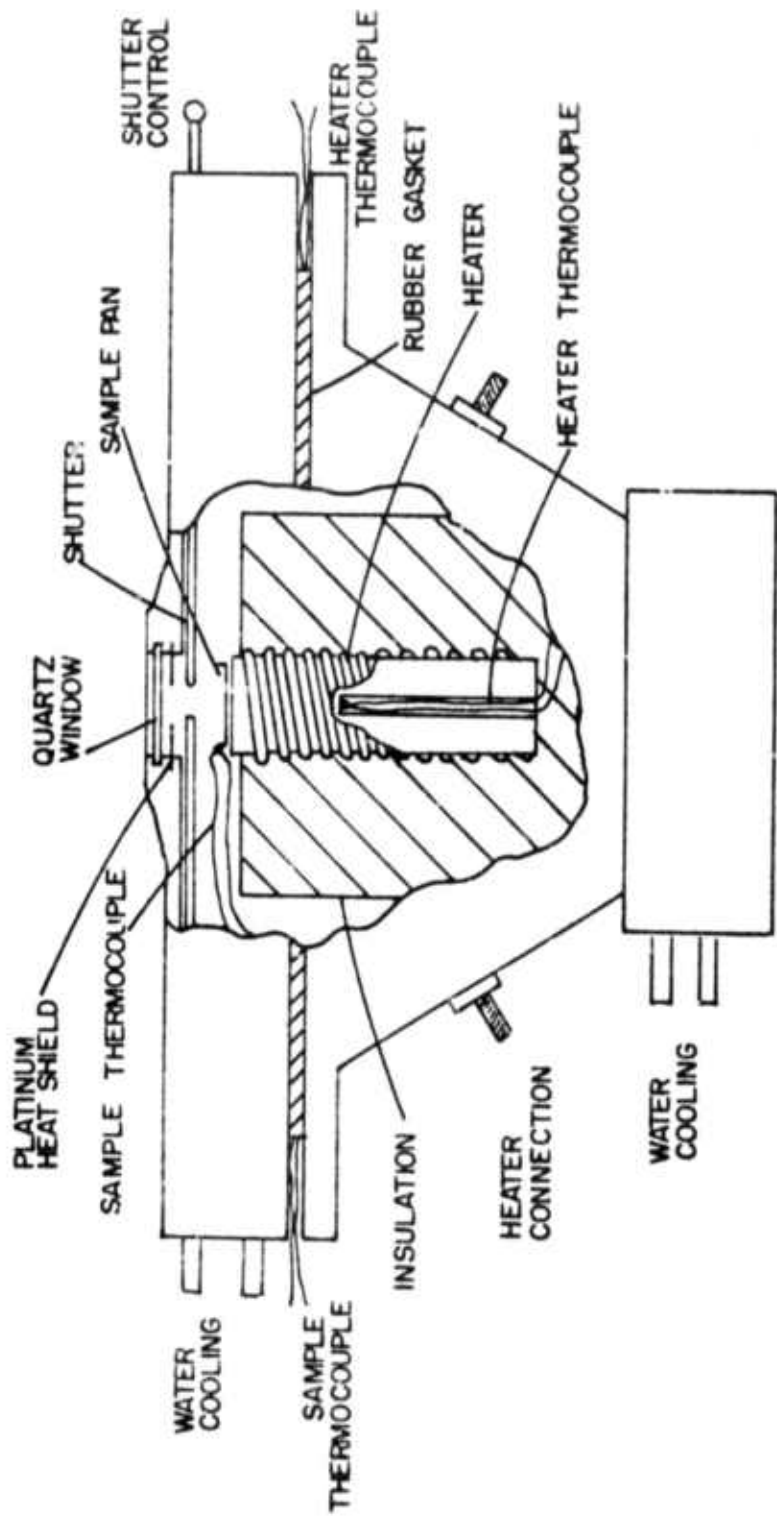


Figure 5  
Metallograph Hot Stage

platinum foil heat shield with a 0.5, cm hole covers a quartz viewing window, 16 mm in diameter and 1 mm in thickness as shown in Figure 5. A shutter is required between the quartz window and the specimen to avoid any organic material or water vapor condensing on the quartz window during the initial heating. The existing shutter mechanism has been modified and now consists of a quartz plate with a 0.5 cm viewing hole that can be adjusted from outside the hot stage. The heat shield, shutter, and distance to the sample holder require a distance of more than 5.8 mm between the sample and the objective and the standard Unitron FF 40x objective with a working distance exactly 5.8 mm cannot be used. Instead, a special focal length lens, Vickers M-028041, is being used. This objective gives a working distance of 14 mm at 20x and permits the use of a Corning water cooled infrared filter between the quartz viewing window and the objective.

### C. Experimental Procedure

#### 1. Resistivity During Firing

The studies of thick film resistor firing are being conducted with samples containing from 5 to 10% RuO<sub>2</sub> (95-90% glass). This range is being used because; (1) it is a test of the sintering model. If the RuO<sub>2</sub> powder was uniformly dispersed in the glass at these low concentrations the resistor would not be electrically conductive because the particles would be separated from one another by distances greater than 1  $\mu$ m. Therefore, the fact that a continuous conductive network is created during firing means that a sintering process such as has been proposed must be responsible for the observed characteristics; (2) the resistance during firing is typically low enough for easy measurement with the

system described earlier; (3) resistors with this concentration have demonstrated an elaborate set of characteristics (e.g., changing resistance and TCR) that are repeatable in sequence although the rates of change are dependent on firing temperature. Previous experiments with high RuO<sub>2</sub> concentrations (40-50%) and low resistance values were affected by firing to a much smaller degree.

The resistor inks used for these samples were blended on the three roll mill [3], and use 5% ethyl cellulose and butyl carbitol screening agent discussed earlier [2]. All samples discussed were screened on a manual machine, but future samples will be prepared on the semi-automatic machine so that more quantitative comparisons can be made among samples [4]. All samples were dried to remove the screening solvent and then fired under a variety of time-temperature conditions with continuous or continual measurements of resistance and temperature as discussed below.

## 2. Surface Tension

The surface tension of the glass is measured by heating several grams of glass in the platinum crucible of Figure 3 until thermal equilibrium is reached, raising the crucible and furnace with the lab jack until the bottom edge of the platinum cylinder is below the surface of the glass, and then slowly lowering the furnace to form a miniscus of glass above the melt. The downward force on the cylinder caused by the raised glass is recorded on a chart until the cylinder breaks away from the glass. The weight of the cylinder and any glass retained on the rim of the cylinder are substracted from the terminal force before breakaway to obtain the force required for the surface tension measurement. Two glasses have been measured. Preliminary measurements were done on a PbO-14.92% SiO<sub>2</sub>

glass in order to verify experimental technique by comparison with previously reported values for  $\text{SiO}_2$  glasses [5]. Then, measurements were carried out with the lead borosilicate glass that has been used in other experiments (62.2%  $\text{PbO}$ , 24.4%  $\text{B}_2\text{O}_3$ , 12.3%  $\text{SiO}_2$ , 1.0%  $\text{Al}_2\text{O}_3$ , 0.6%  $\text{Bi}_2\text{O}_3$ ) [1].

The separation forces determined with the balance were used to calculate surface tension values from the equation

$$\gamma = \frac{F}{4\pi R} [1 - (2.8284 + 0.6095) \sqrt{\frac{h}{R}} + (3 + 2.58 \frac{h}{R} + 0.371 \frac{h}{R}) \frac{2\zeta}{hR}]$$

which can be simplified to [5]

$$\gamma = \frac{F}{4\pi R} \left( 1 - \frac{2.8284\zeta}{\sqrt{hR}} - \frac{0.6095\zeta}{R} + \frac{3\zeta^2}{hR} + \frac{2.585\zeta^2}{R\sqrt{hR}} + \frac{0.371\zeta^2}{R^2} \right)$$

where

$\gamma$  = Surface tension in dynes/cm

$$h = \frac{F}{\pi R^2 \rho g} = \frac{\omega_{\max}}{\pi R^2 \rho}$$

$F$  = maximum force exerted on the cylinder =  $g \omega_{\max}$

$2\zeta$  = thickness of the cylinder

$\rho$  = density of the glass

$R$  = mean radius of the cylinder

$\omega_{\max}$  = maximum pull (gms) exerted on the cylinder

The high temperature density values of the lead borosilicate glass were determined by the extrapolation of lower temperature expansion data [1].

#### D. Results

##### 1. Resistivity During Firing

About forty 5-10%  $\text{RuO}_2$  resistor samples have been fired with concurrent

resistance and temperature measurements using a variety of time-temperature profiles. Most samples are not worthy of individual discussion, but taken as a group they have indicated to some degree the variations in time and temperature that result in resistors (electrically conductive and low TCR (e.g.  $< 2$  megohms  $< \pm 400$  ppm/ $^{\circ}\text{C}$ ) and have shown that the firing process and the creation of a conductive network has certain repeatable characteristics regardless of other minor details. Some of these characteristics can be demonstrated with sample 35, fired at  $590^{\circ}\text{C}$  for 550 hours. The sample was quenched frequently during the firing procedure in order to measure room temperature resistance and TCR and to look for the characteristic symptoms of network formation discussed below.  $R_S$  in Figure 1 was set to 1 megohm and the oscillator was set so that the resistance chart recorder was on scale for an infinite resistance sample. Under these conditions the accuracy in resistance is approximately  $\pm 5\%$  for a sample resistance of  $\leq 100\text{K}\Omega$ ,  $\pm 8\%$  at 1 megohm and  $\pm 15\%$  at 10 Megohms.

Figure 6 shows the approximate room temperature ( $50^{\circ}\text{C}$ ) resistance versus total time at  $590^{\circ}\text{C}$  and clearly shows the formation of a conductive network between 30 and 100 hours, a minimum resistance of  $300\text{K}\Omega$  at 150 hours, and then a gradual increase in resistance up to 350 hours. Figure 7 shows that the hot TCR ( $50^{\circ}\text{C} - 130^{\circ}\text{C}$ ) throughout this period was approximately  $-200$  ppm/ $^{\circ}\text{C}$ . Between 330 hours and 430 hours a significant change occurred. The resistance decreased by a factor of about five and the TCR increased to a positive value.

Figure 6 also shows the resistance of the sample at  $590^{\circ}\text{C}$ . This temperature is high enough for the resistance of the glass to be measured with the measurement system; it is approximately 3 megohms as taken from the measured resistance at the beginning of the experiment. The resistance

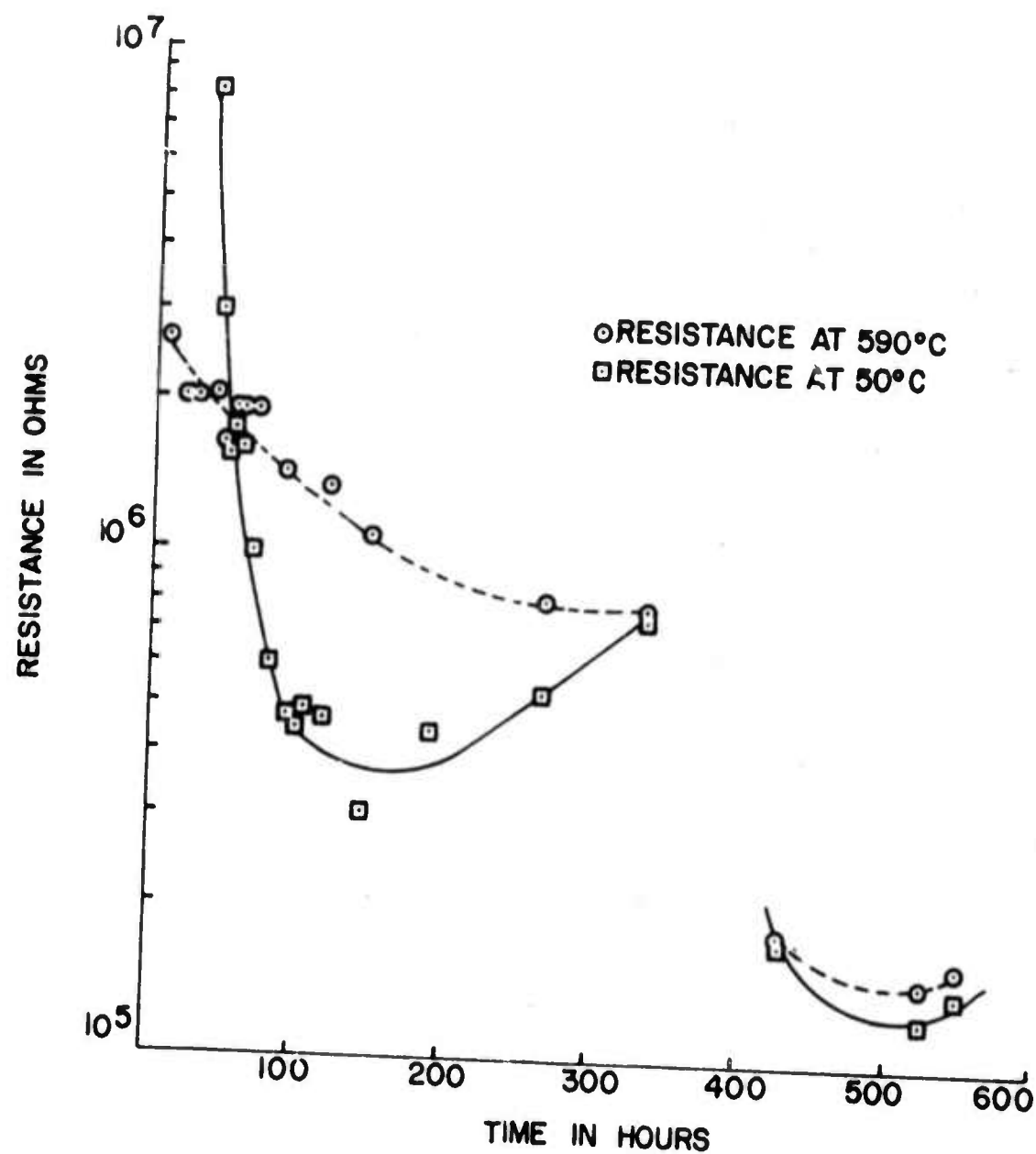


Figure 6  
Resistance versus Time of Sample 35

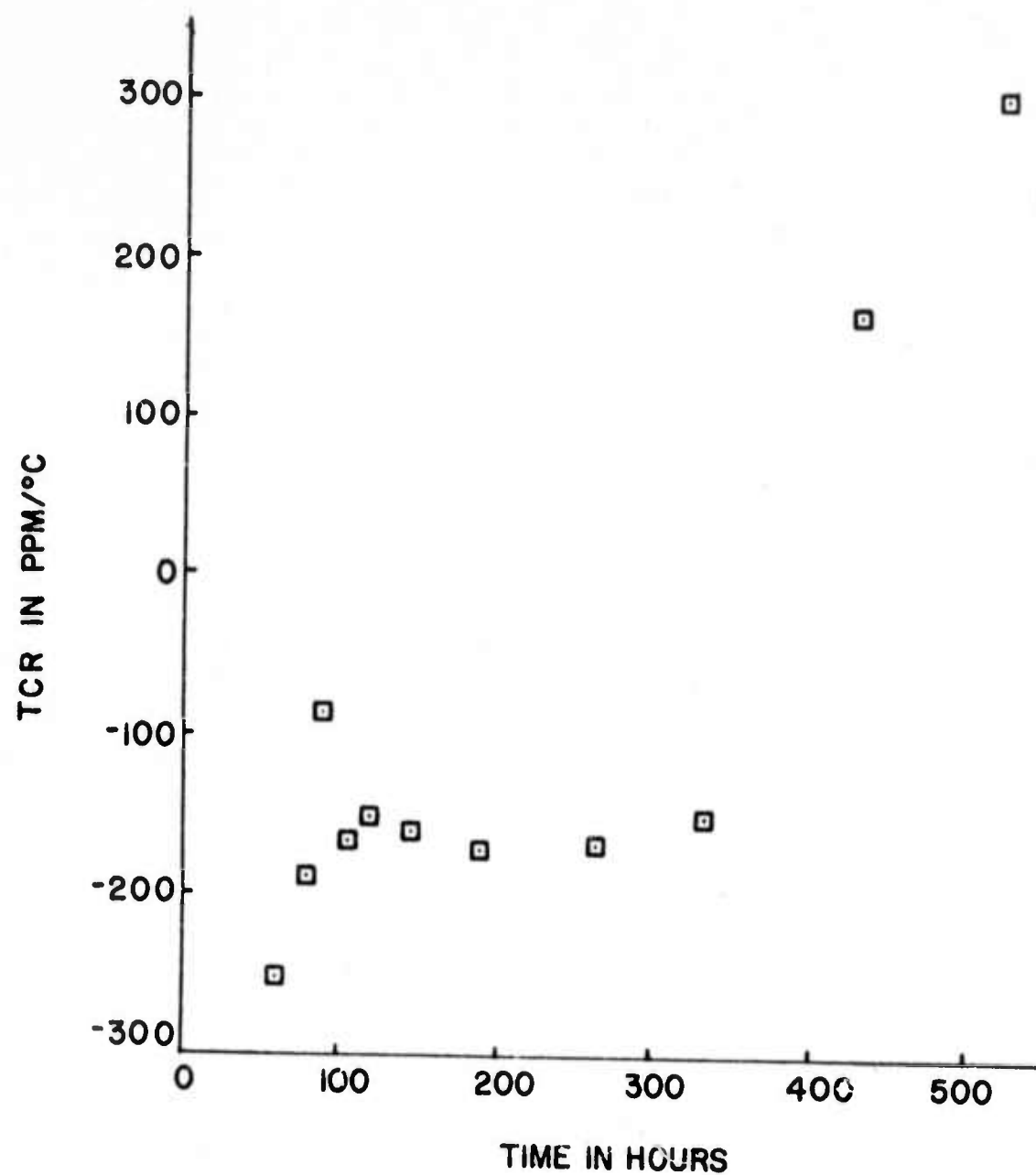


Figure 7

TCR versus Time of Sample 35

at  $590^{\circ}\text{C}$  monotonically decreased by a factor of four during the first 350 hours. At temperatures higher than  $590^{\circ}\text{C}$ , where the resistance of the glass is even lower, the change in resistance during the period of firing was less than observed at lower temperatures and, in general, the resistance at high temperature cannot be used as an indicator of network formation. For example, the two resistance graphs intersect at about 50 hours and the resistance at  $590^{\circ}\text{C}$  is not affected by the room temperature minimum at 150 hours or the subsequent increase. The high temperature resistance for times greater than 400 hours is significantly different; its magnitude is lower and it follows the room temperature resistance more closely.

The resistance versus extended temperature changes during the formation of the conductive network; Figure 8 shows the sequence. Before the network begins to form the glass furnishes the only conduction mechanism, probably ionic. This is shown in Figure 8a after 20 hours of firing time where the resistances during both heating and cooling increase rapidly at lower temperatures. At 26 hours Figure 8b shows a resistance versus temperature behavior that appears to be a characteristic of network formation as a decreasing resistance measured at room temperature. During the heating portion a dip in the graph develops at a temperature a little lower than the softening temperature of the glass. Later, at 42 hours, (Figure 8c), when room temperature resistance measurements indicate that the network is more completely developed, the dip that existed at 26 hours has become more apparent because the resistance at lower temperatures is lower, and because a "bump" has formed at a slightly higher temperature. Also, at this stage of development a dip now appears during the cooling period. Still later in resistor formation, for example,

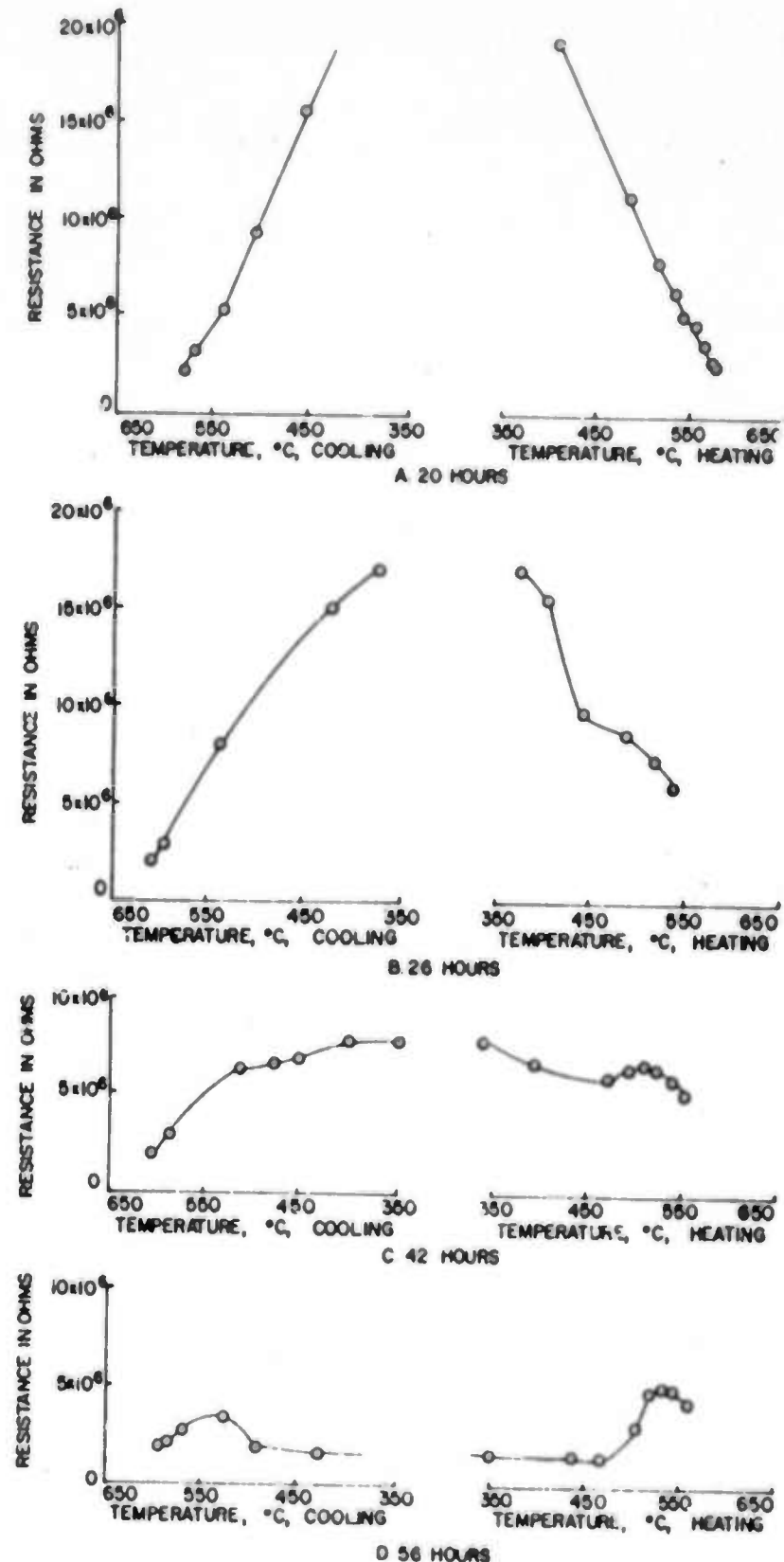


Figure 8

Temperature and Thermal History Dependence of Sample 35

56 hours, dips and bumps exist in both the heating and cooling profiles, but they are always more pronounced in the heating cycle. Figure 8d does not emphasize the magnitude of the dip because it is located near the zero of a linear axis. Not only are the dip and bump characteristic of screen printed resistors, they have also been observed in the firing of bulk samples of  $\text{RuO}_2$  and glass powder [1], and in measurements of the contact resistance between two single crystals of  $\text{RuO}_2$  in the presence of glass [3]. The resistance versus temperature for times greater than 400 hours is not shown in Figure 8, but it remains essentially constant over all temperatures  $< 600^\circ\text{C}$ , changing only a small amount corresponding to a temperature coefficient of several hundred parts per million.

Proper correlation of the proposed sintering model to the behavior of resistors during firing will require further study, but the characteristics of sample 35 are compatible with the basic model. The decrease in resistance during the first 150 hours would represent the coalescence and partial sintering of the  $\text{RuO}_2$  particles initially on the surface of glass spheres, and the increase in resistance from 150 to 350 hours would represent modifications in the network due to densification or to the Ostwald ripening process during which interfacial energies cause the larger particles of  $\text{RuO}_2$  grow as the smallest are dissolved. If the  $\text{RuO}_2$  particles did not sinter completely during the first 350 hours, at lower temperatures interfacial forces would still hold the  $\text{RuO}_2$  in close enough contact for conduction (tunneling, conducting glass near the particle, actual contact, etc.), but at higher temperatures changes in interfacial forces and increased thermal energy would permit a small but critical separation of the particles. The more constant values of lower resistance with positive

values of TCR at times beyond 350 hours are consistent with a sintered network of  $\text{RuO}_2$  particles that is no longer influenced by the condition of the glass matrix.

It had been anticipated that it would be possible to occasionally quench samples during the firing process in order to determine the information such as shown in Figures 6, 7 and 8 without modifying the microstructure development. Presumably the quenching would freeze all microstructural units in place and reheating would simply allow a continuation of the network formation, especially since the heating and cooling times can be made small compared to total firing time at high temperature. Figure 8, with non-repeatable behavior on heating and cooling shows that this is not the case. It has also been observed on several occasions that changing the frequency of heating and cooling cycles, for example from every 20 minutes to every 30 minutes of high temperature firing, influences the average rate at which the network forms. Fortunately, however, the resulting resistors are quite similar even though varying amounts of total firing were required to form the resistor. Thus, a procedure has been developed for preparing a sequence of samples in predictable advancing states of development for observation with optical microscopes and the scanning electron microscope in order to better analyse the formation of the desired microstructure.

## 2. Surface Tension

The surface tension results obtained with the apparatus of Figure 3 for a  $\text{PbO-14.92\% SiO}_2$  glass are shown in Figure 9 along with previously reported data [5] for two glasses having compositions on either side of the one measured. The surface tension versus temperature follows a typical

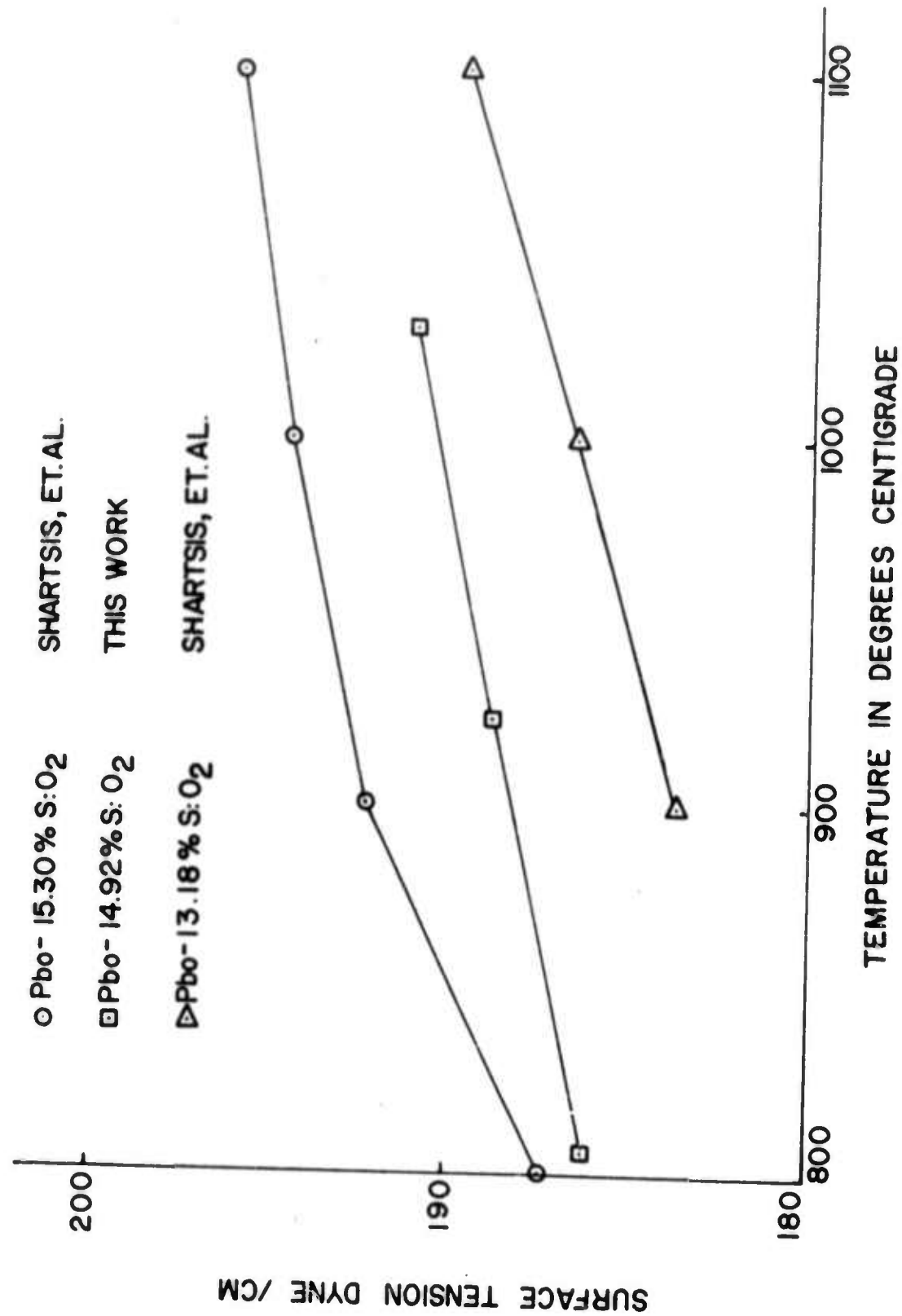


Figure 9

Surface Tension of Lead-Silicate Glass

linear form and is seen to be in good agreement with the previously reported results, indicating proper measurement technique.

The surface tension of the  $\text{PbO-B}_2\text{O}_3-\text{SiO}_2$  glass used for resistor fabrication is shown in Figure 10 over a larger temperature range. The magnitude is typical of that previously reported for similar glasses [5]. The temperature dependence of the surface tension is not linear, but the change amounts to only 10% over the temperature range. A negative temperature coefficient of surface tension had been previously reported [5] for  $\text{PbO-B}_2\text{O}_3$  glasses having 50-80% PbO.

The effects of surface tension have been demonstrated on a qualitative, but dramatic level during the resistor firing experiments. Several samples, particularly those with 5%  $\text{RuO}_2$  content when fired to high temperature developed a characteristic at the interface of the resistor and conductor that consisted of a noticeably reduced thickness and reduced content of  $\text{RuO}_2$ . An example of this is shown in Figure 11a in which the relative lack of the dark  $\text{RuO}_2$  is obvious from the photomicrograph. The reduced thickness is apparent from direct visual observation and was verified with a profilimeter. This phenomena produced a severe problem because samples would appear to be open circuited or very high in resistance when the bulk of the resistor was otherwise normal. The depletion of glass at the interface could easily be explained by the previously observed affinity of the conductor paste for the glass. This can be seen in Figure 11a where the glass has diffused much farther into the conductive than it has across the surface of the substrate. The initial dimension of the resistor can be seen by the black area on conductive; the  $\text{RuO}_2$  does not propagate through the conductive.

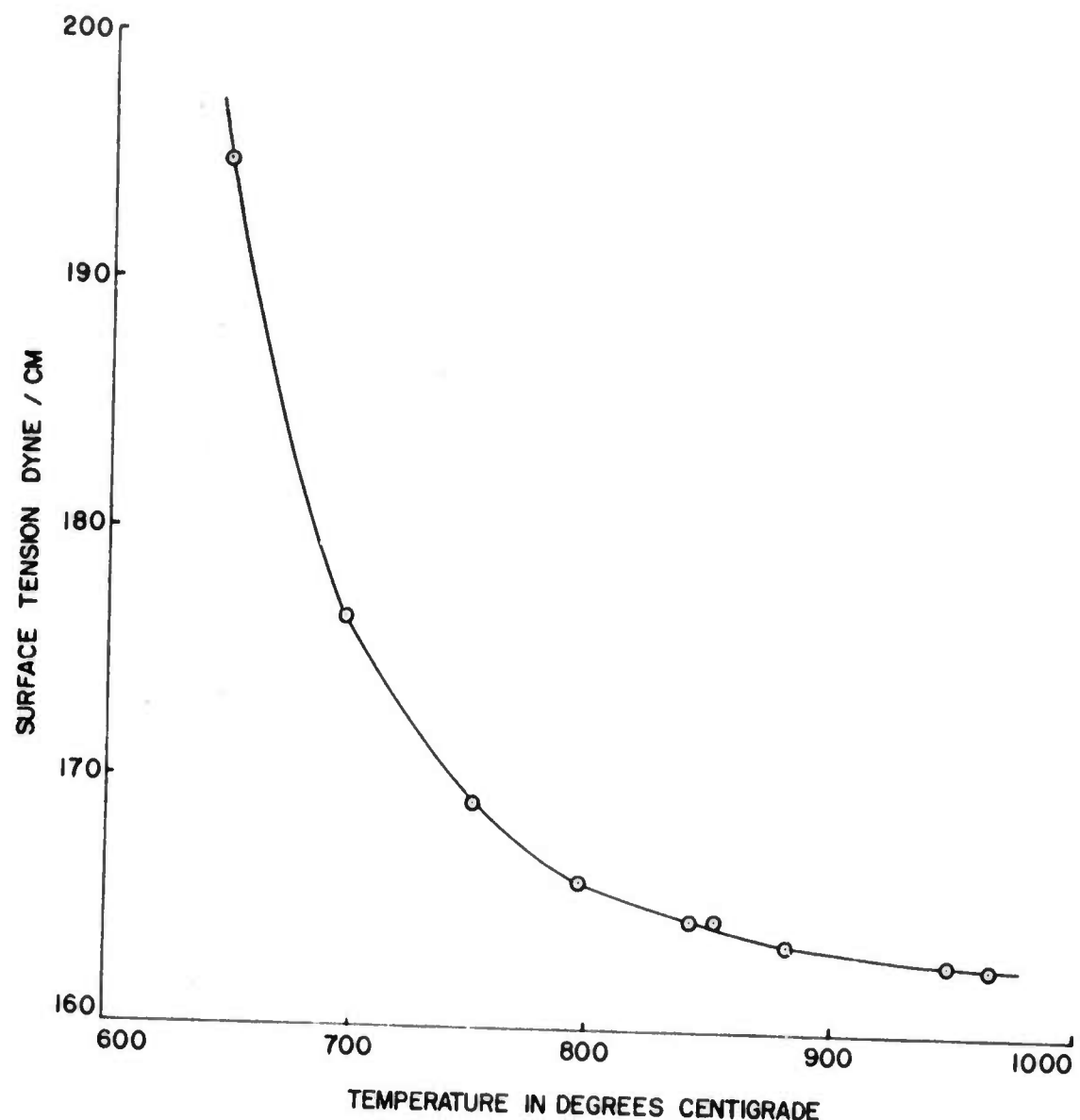
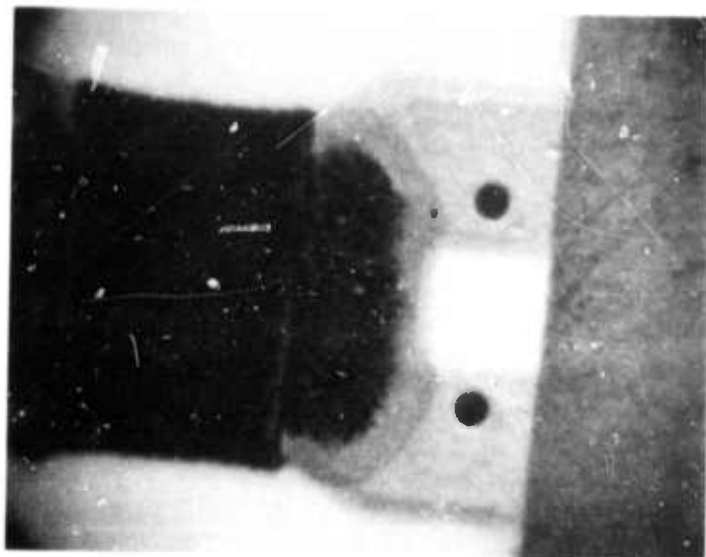
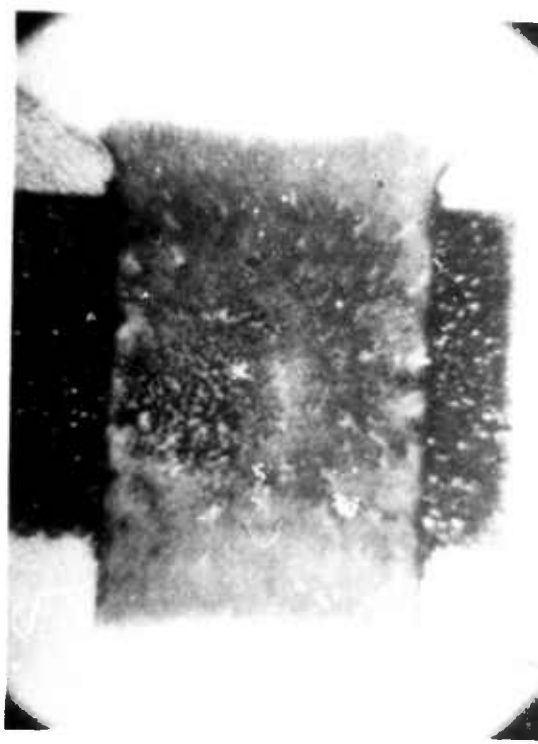


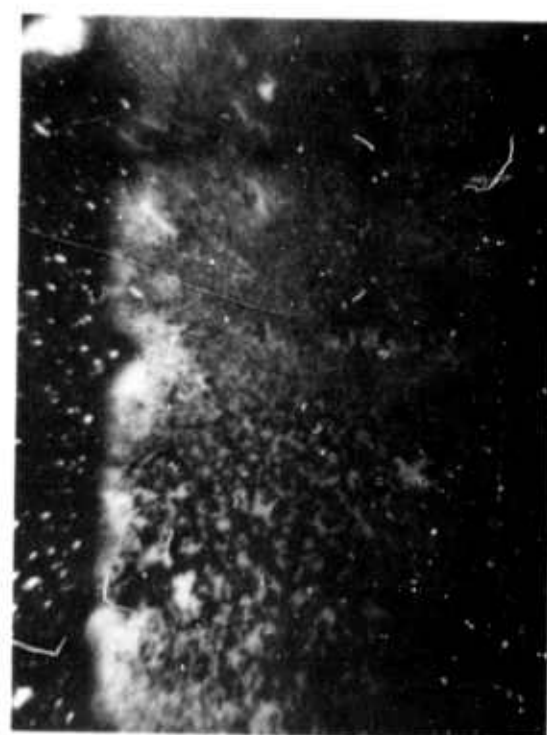
Figure 10  
Surface Tension of Lead Borosilicate Glass



a. Resistor-Conductor Interface



b. Addition of  $\text{Bi}_2\text{O}_3$



c. Addition of  $\text{Bi}_2\text{O}_3$

Figure 11. Effects of Surface Tension on Resistor Formation

The reduced concentration of  $\text{RuO}_2$  at the interface must be due to some phenomenon in addition to the diffusion of glass into the conductive because the opaqueness is less than can be explained by the reduced thickness of the glass. In addition to platinum the primary ingredient in the paste is  $\text{Bi}_2\text{O}_3$  [1] which acts as a flux to improve adhesion. It is a glass former not present in the resistor glass and could, therefore affect the properties of the resistor glass.

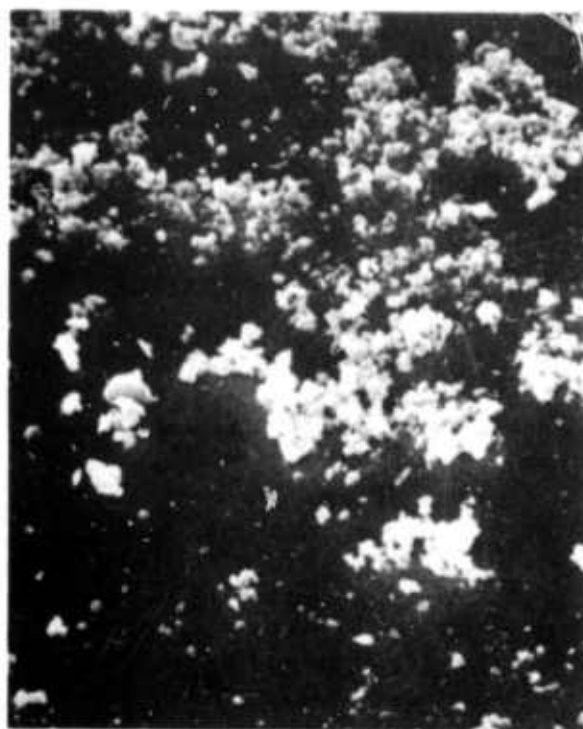
Figure 11b and c show the effect of adding  $\text{Bi}_2\text{O}_3$  to the surface of a resistor. The quantity added was not weighted but it was a particle about 0.8 mm in diameter. The large dark area near the left edge of the resistor (Figure 11b) shows where the particle was placed, the strongly affected area is much larger than the initial particle size. However, the influence of this small amount of  $\text{Bi}_2\text{O}_3$  has extended to some degree throughout the entire resistor as can be seen by the radial pattern of small dark spots and "white tails", regions of glass void of  $\text{RuO}_2$ . Figure 11c shows greater detail in the darkened spot. Although most of the resistor is uniformly dense at this magnification the effected area is characterised by non-uniform agglomeration of the  $\text{RuO}_2$ .

Subsequent work has shown that this interface problem can be avoided if the conductive is first coated with an  $\text{RuO}_2$ -glass ink containing 80%  $\text{RuO}_2$ , but the catastrophic effects on the conductive network from a surface active agent such as  $\text{Bi}_2\text{O}_3$  have far-reaching implications. Quality control becomes much more important in that changes in impurity content of starting materials or substrates previously considered unimportant may be significant if the impurities are surface active.

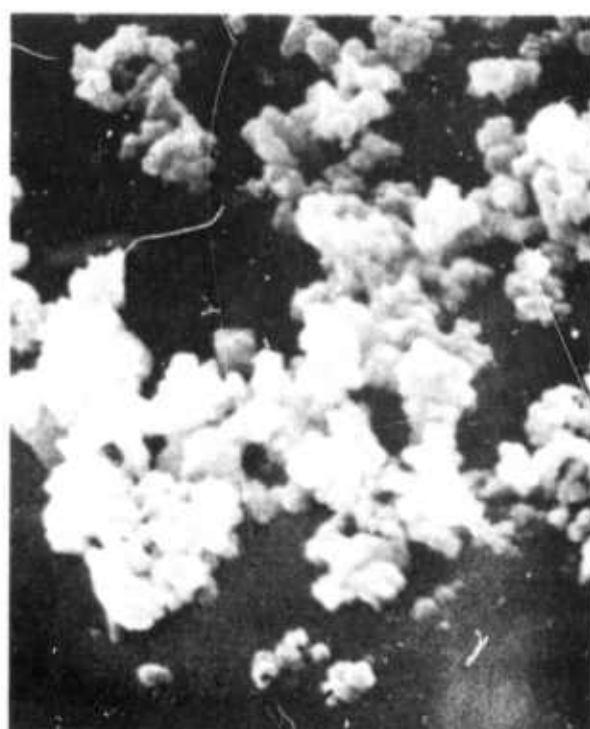
### 3. SEM Studies

Some examples of resistor microstructure obtained with the scanning electron microscope (SEM) are shown in Figure 12. The resistors were etched with HCl to remove the lead from the surface of the glass as previously described [4]. The glass below the surface of the photographs still contains lead and is therefore opaque. As with the optical micrographs discussed in the preceding report [4], a microstructure of interconnected loops of sintered RuO<sub>2</sub> particles as predicted by the sintering model can be observed.

Many of the loops appear to be unconnected because they do not lie in the plane of the photograph, and hence part of them is obscured by the opaque, lead containing glass. The smallest particles ( 0.1 $\mu$ ) show the greatest degree of sintering as predicted from the rate equations.



a. 3000x



b. 10,000x



c. 20,000x



d. 10,000x

Figure 12. Scanning Electron Micrographs of Etched Resistors

### III. Screening Agent Removal

#### A. General

Screening agents are organic liquids blended with the glass and other inorganic powders so that the resulting formulation or ink will have the proper rheological characteristics to be deposited onto the substrate in the desired patterns. Screening agents usually consist of at least a polymer dissolved in a solvent so that the films can be dried to be mechanically durable. Presumably after deposition all of the organics are removed by evaporation, decomposition, etc. However, to say that the screenings agent's only contribution to the manufacturing process is to facilitate printing is, in general, an oversimplification because the polymer may not have been completely removed at temperatures where the glass begins to sinter and/or the polymer must leave by a decomposition process that may require oxygen. It is easy to envision conditions in which some of the oxygen required for the decomposition reaction would come from inorganic compounds in the film thereby changing the composition of the film. It is possible that some commercial thick film inks are characterized by these forms of non-ideality and, in fact, were developed to be optimum in performance when the screening agent does interact with the inorganic materials during firing. That would explain why best results are sometimes obtained when the kilns are fumed to some degree; that is, the atmosphere is purposely contaminated with organic vapors to reduce the oxygen partial pressure at the surface of the film being fired.

Because of the chemical complexity of commercial screening agents and the lack of available information concerning their precise chemical composition, a chemically simple screening agent was developed for this work. It consists of 5<sup>w/o</sup>, N-300 ethyl cellulose dissolved in butyl carbitol, and has been demonstrated as being adequate in printing and drying performance. The purpose of this work is to more quantitatively describe the drying procedure and removal of the ethyl cellulose in order to establish trying procedures which guarantee that no organic materials remain in the films during firing.

#### B. Apparatus

In order to determine the rate of organic removal, a double pan TGA system was constructed that enables accurate, simultaneous measurements of both sample weight and temperature. The basic system, shown in Figure 13, consists of two identical pans symmetrically located in a furnace. The sample pan is attached to an automatic, recording Ainsworth microbalance which, with the sample suspended in air, has an accuracy and resolution capability of about 50  $\mu\text{g}$  and an automatic range of 100 mg. All weight changes are detected by a linear variable differential transformer (LVDT), and recorded as a function of time. The second pan is rigidly attached at the same height as the sample pan and a small thermocouple is located adjacent to the duplicate sample to determine the temperature of the sample on the balance pan. Previous tests with various samples and heating rates have shown temperature agreement between the two pans to be within 4<sup>o</sup>C. A thermocouple cannot be used on the balance pan during weight measurements because the stiffness of the thermocouple leads from the crucible or hangdown wire to the walls of the system would cause unacceptable errors in weight measurements.

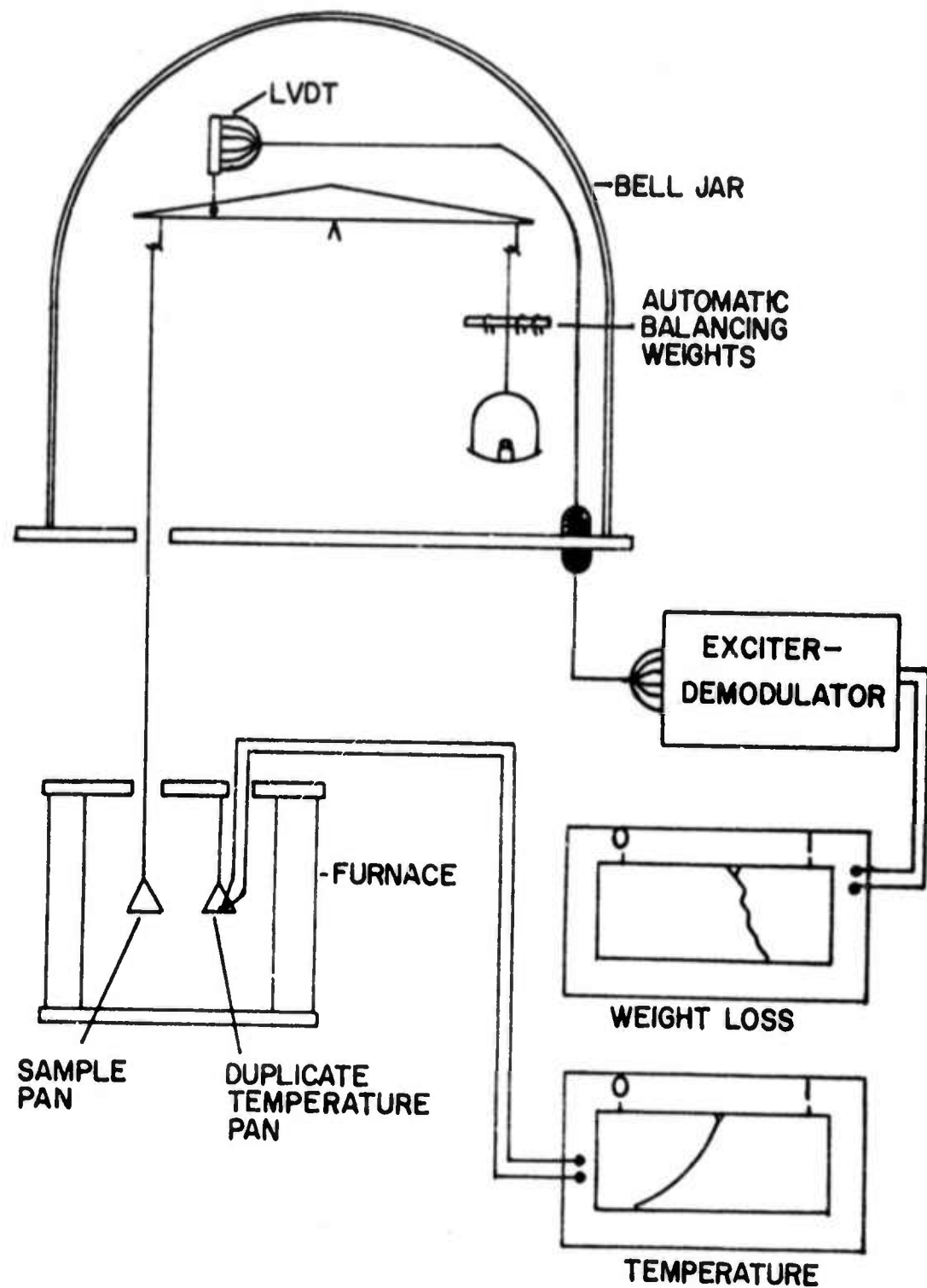


Figure 13

Thermogravimetric Analysis Apparatus

### C. Procedure

The most meaningful form of weight loss experiment would be with films screen printed onto substrates. However, it is not possible to measure the removal of the last few percent of screening agent, the quantity that is of greatest interest. Consequently, all weight loss measurements were carried out with approximately 40 mg of formulation in small crucibles, 7 mm ID and approximately 10 mm high. The materials investigated by TGA were: (1) butyl carbitol solvent; (2) the screening agent; and (3) screening agent plus 40% glass powder (the inorganic content of all printing inks used in other experiments). Evaporation measurements were made under both isothermal and constant heating rate conditions, and in the case of liquid samples, (1) and (2) above, it was possible to determine evaporation rates per unit surface area.

### D. Results

Evaporation studies were begun with the volatilization of the solvent. For a liquid in equilibrium with the gas phase the kinetic theory of gases gives the evaporation of the liquid as

$$\mu = P \left( \frac{M}{2\pi RT} \right)^{\frac{1}{2}} \text{ gm/cm}^2 \cdot \text{sec} \quad (1)$$

where  $P$  is the vapor pressure and  $M$  is the molecular weight of the gas. The Clausius - Claperon equation relating vapor pressure and temperature,

$$\frac{d \ln P}{dT} = - \frac{L}{RT^2}$$

where  $L$  is the latent heat of vaporization, can be integrated to

$$P = Ae^{-L/RT}$$

(3)

where A is the constant of integration. Substituting Equation (3) into Equation (1) gives

$$\mu = Ae^{-L/RT} \left( \frac{M}{2\pi RT} \right)^{1/2}$$

(4)

which can be rearranged into the form

$$\ln (\mu T^{1/2}) = \frac{-L}{RT} + \frac{1}{2} \ln \left( \frac{A^2 M}{2\pi R} \right)$$

for a graphical determination of the constants L and A; a plot of  $\ln (\mu T^{1/2})$  versus  $1/T$  should be a straight line with a slope of  $-L/R$  and an intercept of  $\frac{A^2 M}{2\pi R}$ . Figure 14 shows the isothermal evaporation rates of butyl carbitol at constant temperature plotted in the form of equation (5) for temperatures low enough for convenient equilibrium conditions, and it can be seen that the solvent evaporates in the predicted manner. However, other measurements have shown that in the presence of ethyl cellulose and glass the evaporation of the solvent does not obey the relationship of equation 5.

Figure 15, shows the reciprocal of the evaporation rate of the solvent at constant temperatures versus percent of solvent remaining, and shows that the rate is constant until the last few percent when the surface area decreases. In an ideal evaporation process a solution of ethyl cellulose and solvent should evaporate at a constant rate equal to the solvent alone until only ethyl cellulose remains, in this case, 5%. However, Figure 15 shows that the presence of the ethyl cellulose decreases the evaporation rate (the graph shows the reciprocal) especially at lower solvent

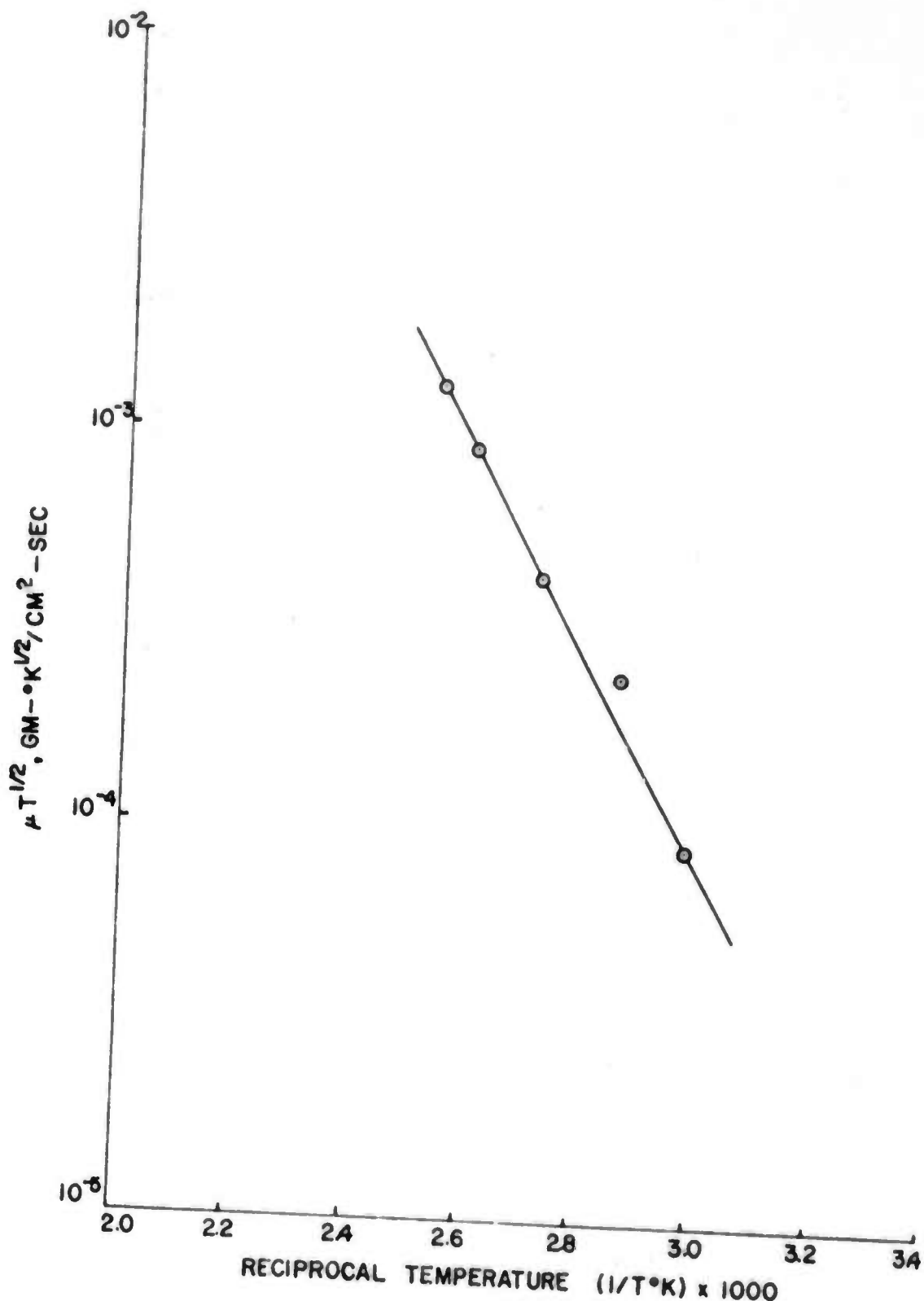


Figure 14

Isothermal Evaporation Rate of Butyl Carbitol versus  
Reciprocal Temperature

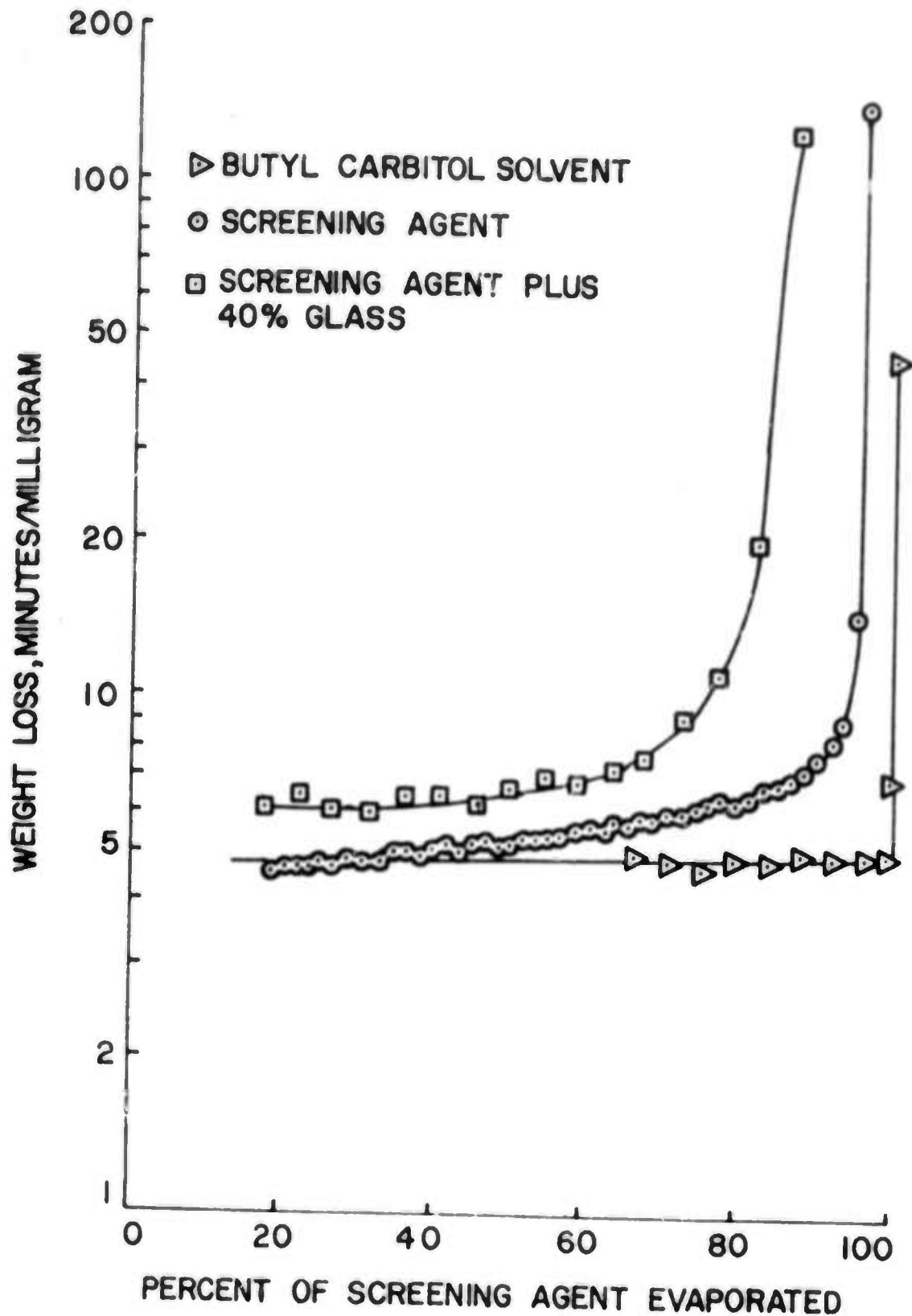


Figure 15

Isothermal Evaporation Rate of Screening Agent

contents. This changing rate could be due to a uniform solution that is not ideal or, more likely, to a dry surface layer of ethyl cellulose that impedes the vaporization. The presence of glass has an even greater effect on evaporation rates; the rate begins to decrease significantly when 50% of the solvent has evaporated.

Because of the dependence of evaporation rates on composition of the formulation it is not possible to fit the data to a simple theoretical expression such as Equation (5), and a detailed, scientific study of the vaporization phenomenon is beyond the scope of this project. Therefore, it was decided to adopt an empirical approach to the development of optimum drying procedures. To this end, a sample of screening agent plus 40% glass was dried at a constant heating rate of  $9^{\circ}\text{C}/\text{min}$ ; the results are shown in Figure 16. The weight indicated is total sample weight including glass. At this heating rate it can be seen that the solvent begins evaporating quickly at about  $150^{\circ}\text{C}$  and evaporates at a nearly constant rate from about  $180^{\circ}\text{C}$  to  $220^{\circ}\text{C}$ . The weight change from  $200^{\circ}\text{C}$  to  $340^{\circ}\text{C}$  represents the loss of the ethyl cellulose. This loss of ethyl cellulose has been studied more carefully to determine the rate of loss. For the small samples of glass and screening agent used for all these experiments the rate increased from about  $25 \mu \text{ gram}/\text{min}$  at  $250^{\circ}\text{C}$  to about  $200 \mu \text{ gram}/\text{min}$  at  $300^{\circ}\text{C}$ . Thus, at  $300^{\circ}\text{C}$  all measurable quantities of ethyl cellulose can be removed in several minutes. Unfortunately, visual observation of the dried samples shows that trace amounts of residue from the ethyl cellulose exist even after very long dryings at  $300^{\circ}\text{C}$ . Temperatures in excess of  $500^{\circ}\text{C}$  are required to remove the last traces of organic residue, but the glass sintering is more rapid than the organic removal at  $500^{\circ}\text{C}$  and above.

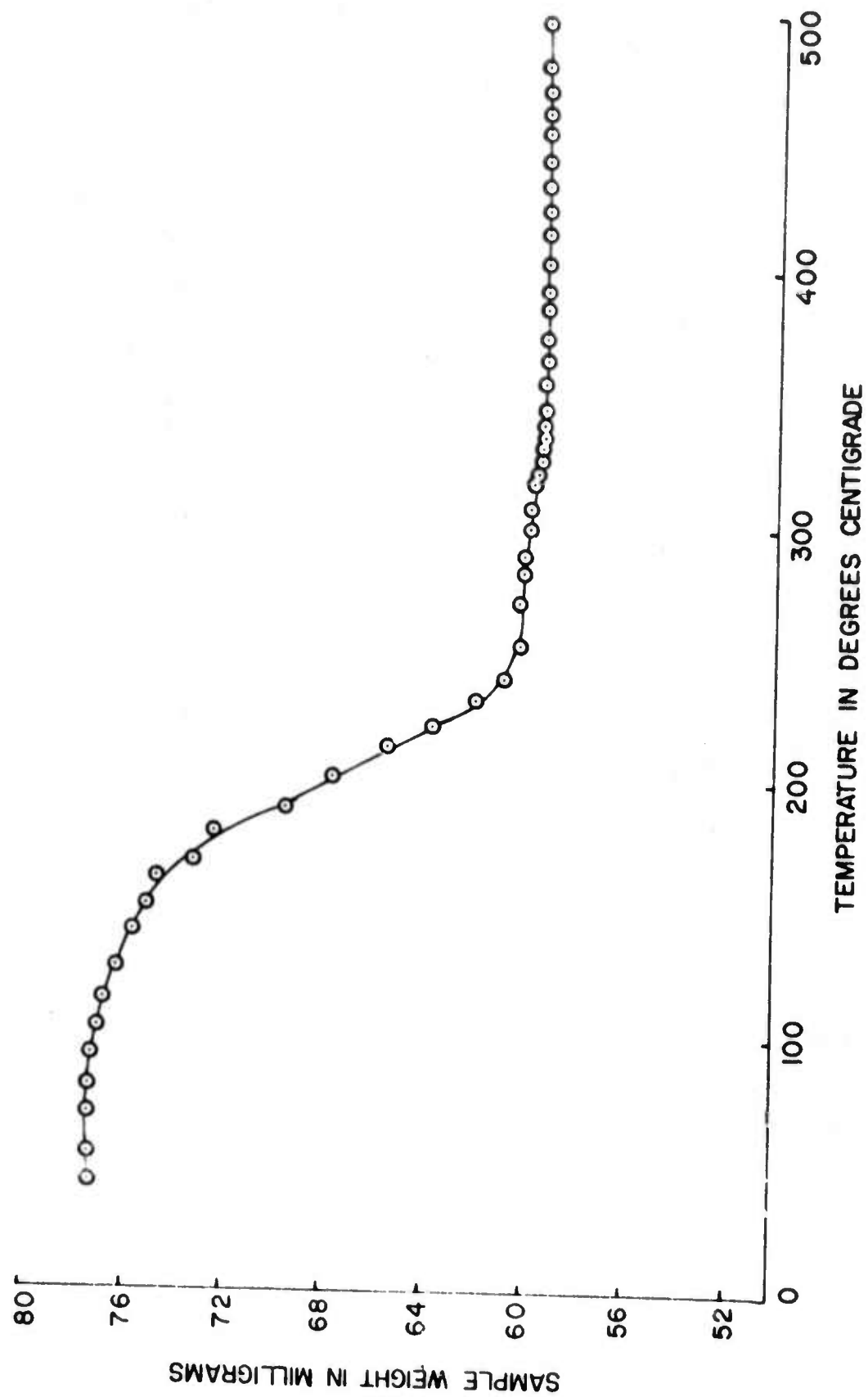


Figure 16  
Evaporation of Screening Agent at Constant Heating Rate

Therefore, although the ethyl cellulose forms a screening agent that is adequate with respect to its rheological characteristics it will yield the situation where some organic material will be present after the glass has flowed; the effect on resistor performance is not known.

## IV RuO<sub>2</sub> Powder

### A. General

Although thick film resistors have been made with ruthenium added by metal resinate and ion implantation, all resistor samples in this program are made with RuO<sub>2</sub> powder. The powder can be made by oxidizing ruthenium metal, but this requires a long time at high temperature (e.g. 2 days at 1000°C [1]), and the resulting particle size is larger than that obtained by other methods. The more desirable method for shorter preparation times and smaller particle sizes is to precipitate a hydrated oxide of small particle size from a soluble salts, and then dehydrate to form the oxide. The general technique, with specific examples, has been discussed by Angus and Gainsbury [6]. They report preparation of the hydrates by precipitating solutions of ruthenium chloride, sodium ruthenate, and ruthenium tetroxide with sodium hydroxide, methyl alcohol, and hydrogen peroxide, respectively. They also report that the temperature of dehydration affects the particle size of the oxide, and that the particle size of the oxide in turn affects the resistivity and TCR of thick film resistors. Heating the hydrate for one hour at 500°C resulted in approximately 0.3μm particles of oxide whereas heating for the same time at 800°C resulted in 1.5μm particles. This comparison is typical and is due to increased grain growth at higher temperatures; the driving mechanism is a reduction in surface area. The effect of the smaller particle size on the properties of the resistor was to decrease both TCR and current noise although the resistivity was unaffected. The properties of resistors should be influenced by the

particle size of the conductive ingredient because of its influence on the development of the conductive network as explained by proposed sintering model. In this case the lower TCR could be due to the increased scattering associated with the smaller particles. Because of these types of interdependencies it is important to adequately characterize the particle size and particle size distribution and to hold these parameters constant by standardizing the method of preparation.

#### B. Experimental Procedure

Since ruthenium dioxide hydrate ( $\text{RuO}_2 \cdot x\text{H}_2\text{O}$ ) is commercially available, quantities were obtained from both Englehard and Mathey Bishop for dehydration to usable oxide. The dehydration is exothermic to the extent that care must be exercised in order to avoid a spontaneous reaction. To plan an appropriate dehydration procedure and to better characterize the hydrate, both DTA and TGA measurements were made during heating. Qualitative DTA results were obtained with a laboratory assembled instrument of standard design, and TGA measurements used the system of Figure 13. In addition to these measurements an electron spectroscopic chemical analysis (ESCA) was done on the surface and a limited number of resistors have been prepared using the dried  $\text{RuO}_2$ .

#### C. Results

The qualitative DTA results, Figure 17, shows that the two hydrates are quite different from one another, probably due to different starting materials and processing conditions. The single peak at  $230^\circ\text{C}$  obtained with the Englehard hydrate and the double peaks at  $186^\circ\text{C}$  and  $285^\circ\text{C}$  with the Mathey Bishop hydrate could represent water loss; this would be

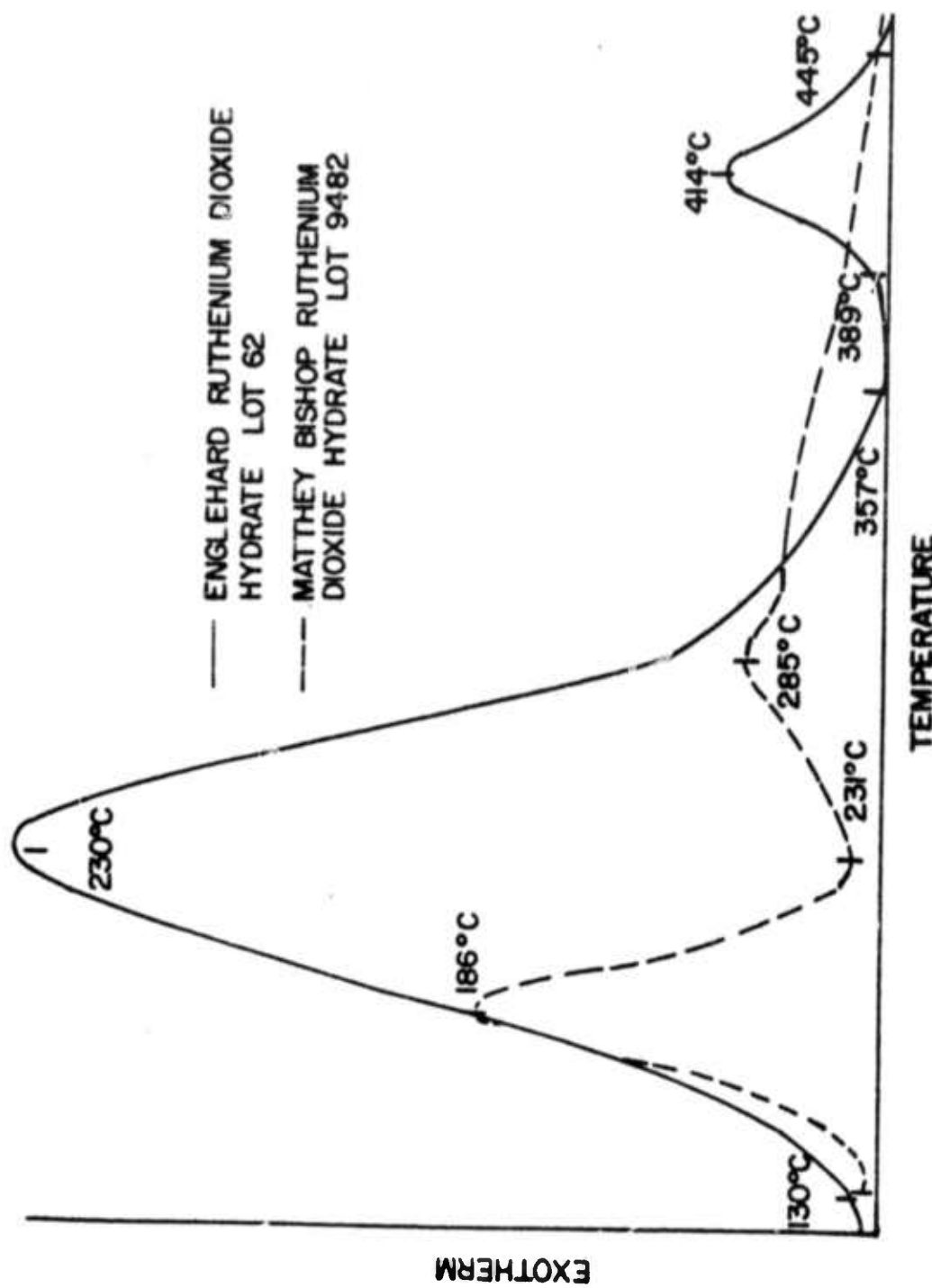


Figure 17

Differential Thermal Analysis of the Dehydration of  $\text{RuO}_2 \cdot x\text{H}_2\text{O}$

typical of dehydration. Although the patterns are of different form and the peak for the Englehard material is much larger, the smaller peaks obtained with the Mathey Bishop hydrate seem to be contained in the larger peak. The exothermic peak at  $414^{\circ}\text{C}$  obtained with the Englehard material is unusually high in temperature for dehydration. This peak may be due to the oxidation of carbon since chemical analysis revealed about 2% carbon in the hydrate. The origin of the carbon is not known, but to be present in such large quantities it would have to have been introduced somewhere in processing, for example from chemisorbed alcohol. The TGA measurements on Englehard hydrate, Figure 18 are not consistent with normal dehydration or with the DTA results since they show a nearly constant rate of weight loss throughout the same temperature range studied by DTA. Although there are regions of changing slope for all three heating rates they do not correspond to the peaks and valleys of the DTA graph. Assuming that all of the weight loss in Figure 18 was due to water, the chemical formula of the hydrate would have had to have been  $\text{RuO}_2 \cdot 2.1 \text{ H}_2\text{O}$ . The TGA measurements do show that adequate drying conditions must be used for complete water removal, however. Only the slowest heating rate,  $1^{\circ}\text{C}/\text{min}$ , was sufficient to achieve complete water removal with a maximum temperature of  $500^{\circ}\text{C}$ . At the more rapid heating rates weight loss is continuing at  $500^{\circ}\text{C}$  and additional time at high temperature would be required for complete water removal. Since TGA measurements during dehydration that have been reported for other hydrate oxides show a rapid weight loss in the temperature range corresponding to an exotherm, the results described here are difficult to interpret. It has been proposed [7] that  $\text{RuO}_2 \cdot x\text{H}_2\text{O}$  is not actually a hydrate but rather very small particles of oxide with chemisorbed

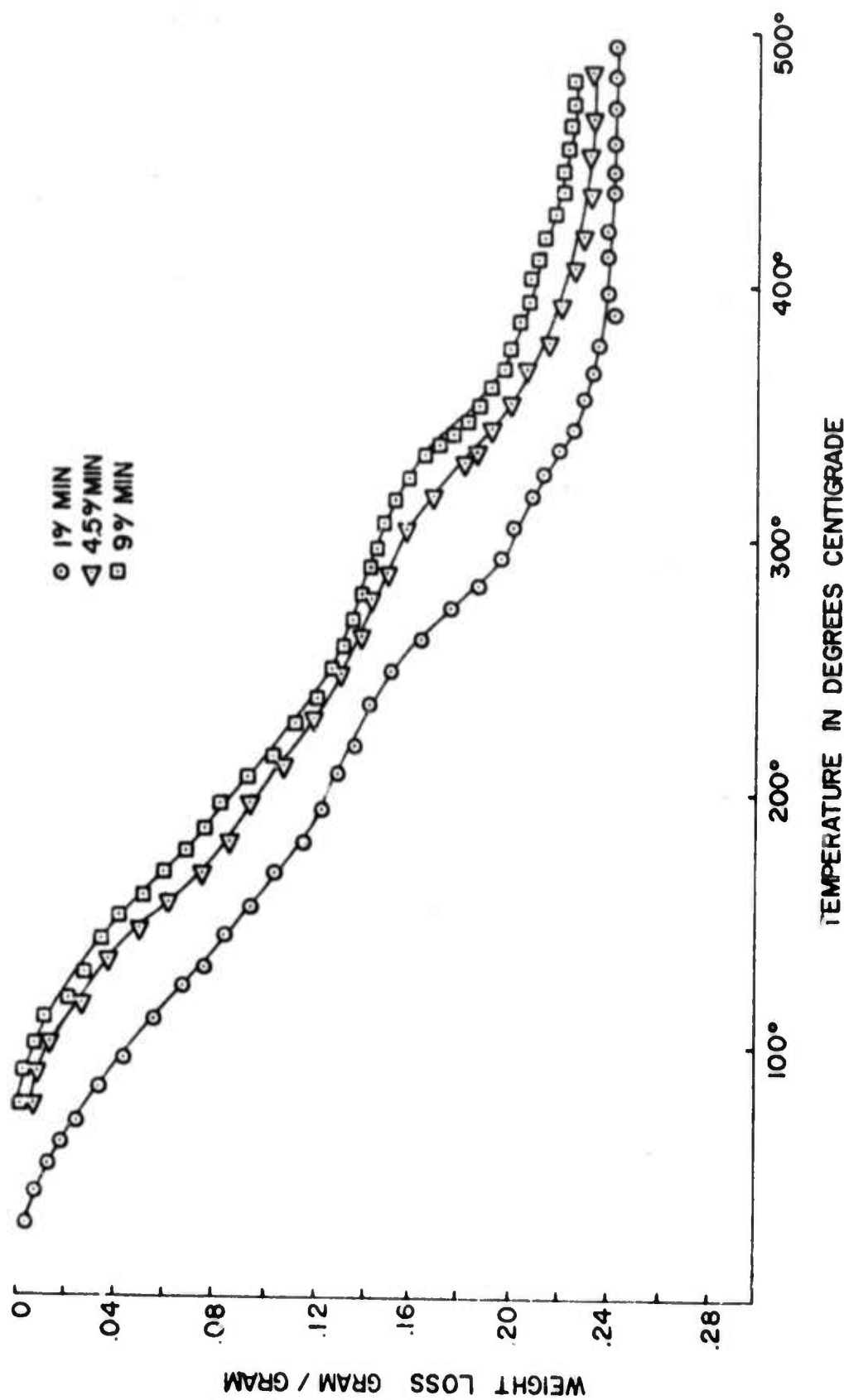


Figure 18

Weight Loss of  $\text{RuO}_2 \cdot x\text{H}_2\text{O}$  at Constant Heating Rate

water on the surface. This could explain the TGA results but not the DTA. Further work will be required for a more complete understanding.

Based primarily on the DTA results a procedure was established for drying the Englehard hydrate in a standard laboratory oven. The temperature is increased every half-hour as follows:

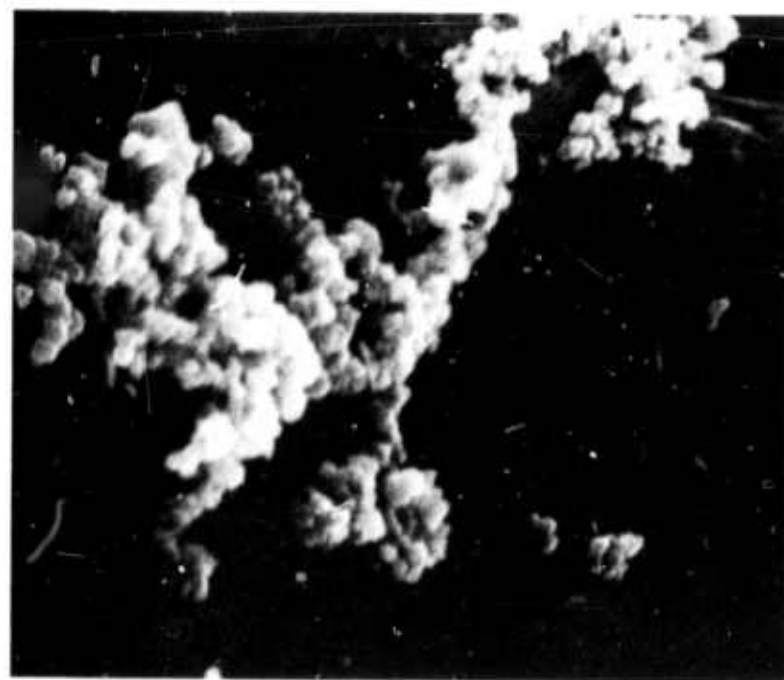
Time = (hrs)	Temp = (°C)
1/2	80
1	95
1 1/2	115
2	120
2 1/2	125
3	130
3 1/2	136
4	150
4 1/2	164
5	180
5 1/2	200
6	230
6 1/2	280
7	330
7 1/2	360
8	400

The majority of individual RuO<sub>2</sub> particles resulting from this drying schedule were in the 0.1 - 1.0 μm size range as shown in the scanning electron micrographs, Figure 19.

To verify that the oxide was suitable for resistors a small quantity of resistor ink was prepared, screen printed and fired at 850°C for 10 minutes. The 18 w/o RuO<sub>2</sub> (82 w/o glass) resistors were approximately



a. Mathey Bishop, 10,000x



b. Englehard, 10,000x

Figure 19. Scanning Electron Micrograph of RuO<sub>2</sub> Powder

276  $\mu\Omega$  and the TCR was about +400 ppu/ $^{\circ}$ C. Although the TCR is higher than desirable overall performance seems adequate considering the arbitrary choice of firing procedure.

## V. Summary and Future Plans

The studies of microstructure development have yielded results in agreement with the predictions of the sequential sintering model, but quantitative correlations await future work.

Studies of screening agent removal uncovered a potential problem area in that the last traces of organic materials are not removed at temperatures below those at which the glass flows. New screening agent systems will be investigated to overcome this problem.

Studies of the drying of ruthenium dioxide hydrate have resulted in some unexpected results, but an empirical procedure has been developed to produce anhydrous RuO<sub>2</sub> in the desired particle size range.

Other studies to be continued or initiated during the coming period include:

### 1. Sintering

The microstructure development during thick film resistor firing which leads to the formation of the physically continuous network of the conductive phase is being studied by hot stage microscopy. The expected sintering mechanisms responsible for the microstructure development have been discussed in detail in a previous report. The general expression for the time dependence of the neckgrowth for the initial stage sintering of two spherical particles of radius a can be given by  $\frac{x^m}{a^n} = Kt$ , where x is the radius of the neck at time t, and K is a constant for the particular system at any given temperature.

The values of m and n for the different sintering mechanisms can be summarized as follows.

	m	n
a. Glass sintering		
Newtonian viscous flow	2	1
b. Conductive sintering		
i) Volume diffusion	5	2
ii) Surface diffusion	7	3
iii) Grain boundary diffusion	6	2
iv) Solution-precipitation		
(a) No Shrinkage	3	1
(b) Shrinkage present.		
i) Rate limiting step is the diffusion flux out of the circular contact area	6	2
ii) Phase boundary reaction leading to solution is the rate limiting step.	4	2

For sintering studies spherical particles of size range  $50-100\mu$  will be used. The glass spheres are prepared by passing the glass particles through the furnace maintained at  $1200^{\circ}\text{C}$  and the  $\text{RuO}_2$  spheres by means of an air grinder from the  $\text{RuO}_2$  single crystals. The growth of the neck between powder particles will be followed continuously at temperature by employing a television camera, a tape recorder and a monitor. Time and temperature will also be recorded simultaneously by means of a separate television camera and a special effects generator.

The important properties of the glass effecting the kinetics of sintering are viscosity, surface tension, and its wettability to  $\text{RuO}_2$ . It has been found that the glass almost completely wets the  $\text{RuO}_2$ . The high temperature surface tension and viscosity are being studied by the "dipping cylinder method" and the "sphere method" respectively.

The neck growth data obtained by sintering of glass spheres will be used to verify that Newtonian viscous flow is the dominant mechanism for

the glass sintering. From the slope of the plot of  $\frac{x^2}{a}$  versus  $t$  and using the experimentally determined values of the surface tension the viscosity of the glass at that temperature can be determined. This value of viscosity of the glass can be compared with the viscosity value determined from the "sphere method". From the neckgrowth data obtained for the conductive sintering, plots of  $\frac{x^n}{a^m}$  versus  $t$  can be obtained for different values of  $m$  and  $n$  and the appropriate sintering mechanisms can be determined. From the slopes of the above plots, the material properties, e.g. diffusion coefficients, contained in the constant  $K$  can be determined. Sintering experiments will also be carried out using  $\text{RuO}_2$  spheres of different particle sizes in order to examine the process of Ostwald ripening which, it is postulated, leads to the discontinuity in the conductive network.

After the kinetic expressions for the isothermal sintering processes have been obtained, the sintering experiments will be carried out on continuous heating employing linear heating rates, and the kinetic expressions will be appropriately modified. From the known values of the surface tension and viscosity of the glass and solubility of  $\text{RuO}_2$  in the glass at different temperatures it should be possible to assess the effect of these variables on the kinetics of sintering.

## 2. Electrical Properties of the $\text{RuO}_2$ -Glass Interface Region

Even though results reported previously indicate that the electrical properties of small particle size  $\text{RuO}_2$  are significantly different from those of massive single crystal  $\text{RuO}_2$ , the differences are not great enough to explain the nearly-zero and sometimes negative TCR observed with thick film  $\text{RuO}_2$  resistors. This phenomenon must be due to an additional effect resulting from the presence of the glass. In order

to better characterize the "contact" resistance between adjacent regions of  $\text{RuO}_2$  in the glass, single crystals of  $\text{RuO}_2$  will be precoated with glass in varying thicknesses and suitable counter electrodes applied. Current-voltage measurements and capacitance measurements as a function of bias voltage will be made in order to determine the mechanisms of charge transport through the glass films.

### 3. Particle Size Effects on the Resistivity of $\text{RuO}_2$

Previous studies on this project indicate that the apparent electrical properties of small particle size ( $50\text{-}100\text{\AA}$ )  $\text{RuO}_2$  may differ from that of the bulk, single crystal values; the electrical resistivity may be greater by a factor of about three and the TCR lower by about the same factor. A possible explanation for these phenomena is that the scattering of the conduction electrons is increased due to increased crystal defects. This increased scattering would increase the resistivity and, since defect scattering has a smaller temperature dependence than phonon scattering, the TCR would be lower. The increased scattering at the surface would be more influential with small particles and, since the smaller particles are prepared at lower temperature, there may be a higher degree of crystal disorder throughout their volume. Thus, the indications that the electrical properties of small size powder are different from those of bulk single crystal are not inconsistent with theoretical properties of materials.

The procedure for determining the resistivity of the powder will be to uniformly disperse the powder in a proper matrix, measure the resistivity of the composite, and apply the proper mixing rules. A review of heterogeneous microstructures and the associated mixing rules shows that for maximum sensitivity to the resistivity of the dispersed phase ( $\text{RuO}_2$ ),

the resistivity of the matrix material should not be greater than ten times the resistivity of the powder. This excludes common dispersants since they are usually high in resistivity, and even liquid electrolytes of strong acids and bases. The only suitable materials in terms of resistivity and ease of handling are moderately low melting temperature alloys such as tin-lead solder and the family of alloys with melting temperatures near 100°C (Wood's metal, Rose's metal, etc.). The dispersing procedure will be to melt the alloy, add the powder, and mix with a propeller while under a vacuum to avoid entrapment of air as a third phase and to minimize oxidation of the alloy.

#### 4. Effects of Substrate Expansion

Substrates with coefficients of linear thermal expansion varying from 2 to  $10 \times 10^{-6}/^{\circ}\text{C}$  have been obtained and flame sprayed with a thin coating of alumina so that the resistor-substrate interface will be the same in all cases. The resistance and TCR of resistors printed and fired on these substrates will be measured and the results analyzed in light of the results obtained with the RuO<sub>2</sub>-glass composites.

#### 5. Test of Models

The sheet resistance and TCR of resistors and conductors will be determined as a function of volume fraction of conductive phase to glass, and as a function of particle size of the conducting phase and of the glass. The important glass parameters (viscosity and surface tension) will be varied at constant thermal expansion, and the results compared with predictions of the microstructure model and the interface model. Chemical additives which will alter the electrical properties according to the interface model, but which will not effect microstructure development will be utilized to further test the interface model.

#### 6. Resistor and Conductor Evaluation

Predictions of the microstructure and interface models will be utilized to develop optimum resistor and conductor formulations within the given materials system. The performance of these will be evaluated according to the list of specifications developed.

## VI. REFERENCES

1. R. W. Vest, Semi-annual Technical Report for the period 7/1/70-12/31/70, Purdue Research Foundation Grant No. DAHC 15-70-67, ARPA Order No. 1642, February 1, 1971.
2. R. W. Vest, Semi-annual Technical Report for the period 7/1/71-12/31/71, Purdue Research Foundation Grant No. DAHC-15-70-G7, ARPA Order No. 1642, February 1, 1972.
3. R. W. Vest, Semi-annual Technical Report for the period 1/1/71-6/30/71, Purdue Research Foundation Grant No. DAHC-15-70-G7, ARPA Order No. 1642, August 1, 1971.
4. R. W. Vest Semi-annual Technical Report for the period 1/1/72-6/30/72, Purdue Research Foundation Grant No. DAHC-15-70-67, ARPA Order No. 1642, August 1, 1972.
5. L. Shartsis, S. Spinner, and A. W. Smock, Jour. Amer. Ceramic Society, 31, 23 (1948).
6. H. C. Angus and P. E. Gainsbury, Elec. Comp., 84, January, 1968.
7. J. M. Fletcher, et.al., J. Chem. Soc. (A), 653 (1968).